

Red Giant Branch stars: the theoretical framework.

Maurizio Salaris

Astrophysics Research Institute, Liverpool John Moores University, Twelve Quays House,
Egerton Wharf, Birkenhead CH41 1LD, United Kingdom; ms@astro.livjm.ac.uk

Santi Cassisi

Osservatorio Astronomico di Collurania, via M. Maggini, 64100 Teramo, Italy;
cassisi@te.astro.it

Achim Weiss

Max Planck Institut für Astrophysik, Karl-Schwarzschild-Str. 1, 85748 Garching,
Germany; weiss@mpa-garching.mpg.de

Received _____; accepted _____

ABSTRACT

Theoretical predictions of Red Giant Branch stars’ effective temperatures, colors, luminosities and surface chemical abundances are a necessary tool for the astrophysical interpretation of the visible–near infrared integrated light from unresolved stellar populations, the Color-Magnitude-Diagrams of resolved stellar clusters and galaxies, and spectroscopic determinations of red giant chemical abundances. On the other hand, the comparison with empirical constraints provides a stringent test for the accuracy of present generations of red giant models.

We review the current status of red giant stars’ modelling, discussing in detail the still existing uncertainties affecting the model input physics (e.g., electron conduction opacity, treatment of the superadiabatic convection), and the adequacy of the physical assumptions built into the model computations.

We compare theory with several observational features of the Red Giant Branch in galactic globular clusters, such as the luminosity function ‘bump’, the luminosity of the Red Giant Branch tip and the envelope chemical abundance patterns, to show the level of agreement between current stellar models and empirical data concerning the stellar luminosities, star counts, and surface chemical abundances.

Subject headings: atomic processes – convection – globular clusters: general – nuclear reactions, nucleosynthesis, abundances – stars: atmospheres – stars: evolution – stars: interiors – stars: Hertzsprung-Russell (HR) and C-M diagrams

1. Introduction

The Red Giant Branch (RGB) is one of the most prominent and well populated features in the Color-Magnitude-Diagram (CMD) of stellar populations with ages larger than about 1.5 – 2 Gyr. The theoretical modelling of RGB stars plays therefore a wide ranging role, involving various fields of galactic and extragalactic astrophysics.

Since RGB stars are cool, reach high luminosities during their evolution, and their evolutionary timescales are relatively long, they provide a major contribution to the integrated bolometric magnitude and to integrated colors and spectra at wavelengths larger than about 900 – 1000 nm of old distant, unresolved stellar populations (e.g. Renzini & Fusi-Pecci 1988; Worthey 1994). A correct theoretical prediction of the RGB spectral properties and colors is thus of paramount importance for interpreting observations of distant stellar clusters and galaxies using population synthesis methods, but also for determining the ages of resolved globular and open clusters, by means of isochrone fitting techniques.

The *I*-band brightness of the tip of the RGB (TRGB) provides a robust standard candle, very much independent of the stellar age and initial chemical composition, which can allow to obtain reliable distances out to about 10 Mpc using *HST* observations (e.g., Lee, Freedman & Madore 1993 – LFM93). Due to the lingering uncertainties on the empirical determination of the TRGB brightness zero point, RGB models provide an independent path to the calibration of this important standard candle (Salaris & Cassisi 1997). Also the theoretical calibration of the luminosity of Horizontal Branch (HB) stars and their RR Lyrae population (whose parallax-based distances still show a very large error bar; see, e.g., Groenewegen & Salaris 1999) is dependent on the correct modelling of the previous RGB phase, since HB luminosities (like the TRGB ones) are determined by the value of the electron degenerate He-core mass (M_{core}^{He}) at the end of the RGB evolution.

Predicted evolutionary timescales along the RGB phase play a fundamental role in the determination of the initial He abundance of globular cluster stars through the R parameter (number ratio between HB stars and RGB stars brighter than the HB at the RR Lyrae instability strip level; see, e.g. Iben 1968a, Sandquist 2000, Zoccali et al. 2000), while an accurate modelling of the mixing mechanisms efficient in the RGB stars is necessary to correctly interpret spectroscopic observations of their surface chemical abundance patterns.

These various applications of RGB stellar models to fundamental astrophysical problems crucially rely on the ability of theory to predict correctly:

- the CMD location (in T_{eff} and color) and extension (in brightness) of the RGB as a function of the initial chemical composition and age;
- the evolutionary timescales (hence the relative numbers of stars at different luminosities) all along the RGB;
- the RGB stars’ physical and chemical structure, as well as their evolution with time.

The main goal of this review is to discuss the existing uncertainties in theoretical RGB models, and to assess the reliability of their predictions.

In §2 we present an outline of RGB stellar evolution, while in §3 and §4 fundamental properties of the CMD and luminosity functions of RGB models are reviewed. §5 analyzes the input physics currently used for computing RGB models, and how related uncertainties affect the outcome of the calculations; §6, §7 and §8 discuss observational tests for the accuracy and adequacy of RGB models by employing CMDs, spectroscopic observations, and luminosity functions. §9 reviews the use of the TRGB as standard candle, and conclusions follow in §10.

2. RGB stellar evolution

‘Canonical’ stellar models are usually defined as models computed by solving the equations of stellar structure in the assumption of spherical symmetry (e.g. Kippenhahn & Weigert 1991), neglecting magnetic fields, rotation and mass loss from the surface, considering convection as the only efficient mixing mechanism, and assuming that the convective regions are always fully mixed, their boundaries being fixed by the Schwarzschild criterion. In the rest of this paper we will use the definition ‘non-canonical’ for models computed including additional physical effects like, e.g. overshooting from the Schwarzschild boundary of convective regions or atomic diffusion.

The solution of the stellar structure equations for a given initial value of the total mass and chemical composition provides the run of physical quantities (such as density, radius, pressure, temperature, luminosity) as well as the chemical abundance profiles from the center up to the surface of the star, and their evolution with time. In order to compare theory with photometric observations the stellar evolution results must be then supplemented with some prescriptions to determine bolometric corrections and color indices, all along the evolutionary track.

In the following we present a summary of the RGB stellar evolution (we refer the reader to the seminal papers by Sweigart & Gross 1978 and Sweigart, Greggio & Renzini 1989, 1990 for a detailed discussion on this subject).

2.1. Evolution up to the RGB tip

RGB stars are objects with masses lower than $\sim 2.0 M_{\odot}$ (the precise value depends on the initial chemical composition), which develop electron degenerate He-cores after the end of central H-burning, surrounded by a thick H-burning shell (thickness of the order

of $0.1M_{\odot}$) and a convective envelope whose chemical composition is the initial one. The envelope temperature gradient is to a large extent adiabatic, apart from the most external layers, where it becomes superadiabatic, and must be treated according to some prescribed convection theory.

At this stage, the convective envelope progressively deepens and the H-shell narrows down to a thickness of the order of $0.001 M_{\odot}$, while the star crosses the CMD towards redder colors (i.e. lower T_{eff} and larger radius). There is a large body of literature devoted to the identification of what is (or what are, if more than one) the precise physical reason for the expansion of the star to red giant dimensions (a fact that comes out naturally from the integration of the stellar structure equations), but a general consensus has not been yet reached; we address the reader to the papers by Weiss (1989), Iben (1993), Renzini & Ritossa (1994), Sugimoto & Fujimoto (2000), and references therein.

Due to the steady deepening of the convective region, the lower boundary of the convective envelope enters regions chemically processed (some produced He and the C and N abundances reaching their CN-cycle equilibrium value) by the central H-burning phase; this material is mixed almost instantaneously throughout the convective envelope, thus altering the surface abundances. This phenomenon, called first dredge-up, causes an increase of the surface He abundance, and an increase of the N/C ratio with respect to the original values. Convection reaches its maximum extension (in mass) near the base of the RGB¹, and from this moment on the lower convective boundary slowly recedes towards

¹It is important to remark here that the very deep convective envelope is able to almost completely erase the effect of atomic diffusion – if efficient during the previous main sequence phase – because it reengulfs almost all the material previously diffused out of the narrower convective region (and moreover the RGB evolution is too fast to be itself affected by atomic diffusion). This means that RGB models computed with and without considering

the surface, due to the steady growth of the He-core which accretes He produced by the H-burning shell. The evolution along the RGB covers a relatively small range in T_{eff} (T_{eff} slowly decreasing with time) and a large range of surface luminosity, which increases with time. Due to the growth of $M_{\text{core}}^{\text{He}}$, the H-shell will encounter the sharp discontinuity of the H-profile left at the point of maximum extension of the convective envelope. The star reacts to the sudden increase of available fuel by lowering its surface luminosity and slowing down the evolutionary timescale, before starting again to increase its luminosity after the shell has moved past the discontinuity. This occurrence is recorded in both the differential luminosity function (LF – number of stars in a given brightness interval as a function of the brightness itself) and the integrated LF (sum of the number of stars from an arbitrary origin to a given value of the brightness, as a function of the brightness itself) of old stellar populations as, respectively, a local peak (the so-called RGB bump) in the differential LF, or a break in the slope of the integrated LF. The RGB bump is a genuine prediction of theory (Thomas 1967, Iben 1968b) confirmed many years later by observations of the globular cluster (GC) 47Tuc (King, Da Costa & Demarque 1985).

When $M_{\text{core}}^{\text{He}}$ reaches about $0.50 M_{\odot}$ (the precise value depends weakly on the total mass of the star, being more sensitive to the initial chemical composition), He-ignition occurs in the electron degenerate core, producing the so called He-flash which terminates the RGB phase by removing the electron degeneracy in the core, and drives the star onto its Zero Age Horizontal Branch (ZAHB) location, that marks the start of quiescent central

atomic diffusion are almost indistinguishable (e.g., Proffitt & Vandenberg 1991, Castellani et al. 1997). More in detail, the RGB T_{eff} is basically unaffected by the inclusion of diffusion, the $M_{\text{core}}^{\text{He}}$ values at the TRGB differ by about $0.004 M_{\odot}$ (larger values in the case of models with diffusion), and the TRGB surface He mass fraction is larger by ~ 0.01 in the case of canonical models (Cassisi et al. 1998).

He-burning plus shell H-burning. As an example, Fig. 1 shows the evolution of a $1.0 M_{\odot}$ ($Z=0.0004$, $Y=0.231$) star from the base of the RGB up to the He-flash (Salaris & Weiss 1998 models). The RGB bump region is marked with a circle; the RGB base and the TRGB are also indicated.

Due to the relatively short timescale of RGB evolution (RGB timescales are of the order of a few percent of the main sequence lifetime), the RGB portion of theoretical isochrones (e.g. the CMD locus occupied by stars of different masses with the same initial chemical composition and age) is populated by stars all with almost the same mass. This means that for RGB stars in simple stellar populations (single age, single initial chemical composition), the CMD location and the expected number of stars along the red giant phase provided by an isochrone of a fixed age, are equivalent to the those given by the RGB evolutionary track of the appropriate stellar mass.

2.2. Mass loss along the RGB

Stars along the RGB lose mass from their convective envelope (e.g., Reimers 1975a,b), and the precise amount of mass loss along the RGB is a key parameter which determines color location and extension of the observed HB in GCs. From the point of view of the RGB evolution, however, mass loss (in the case of the rates necessary to explain the bulk of the observed HB stars in Galactic GCs, excluding the stars in the HB blue tails of some cluster, for which very extreme rates must be assumed – see, e.g., Castellani & Castellani 1993, D’Cruz et al. 1996) has a negligible effect on the overall properties of RGB stars. In fact, the stars react on Kelvin-Helmholtz timescales to the surface mass loss, rearranging their radii according to the instantaneous value of the total mass (e.g. Castellani & Castellani 1993); the stellar radius is however very weakly dependent on the value of the mass. The internal structure and evolutionary timescales are always completely unaffected by this process;

this property is due to the fact that the nuclear timescale is significantly longer than the Kelvin-Helmholtz timescale of the envelope thermal readjustment.

A typical value for the mass lost along the RGB in galactic GCs is of the order of $0.20M_{\odot}$ (as inferred from the observed color distribution of stars along the HB of the bulk of GCs); RGB tracks with this mass difference are almost coincident in the CMD. Moreover, the mass loss appears to be also a strong function of the stellar luminosity, so that the bulk of the RGB mass loss happens only close to the TRGB. A very informative summary of the available analytical mass loss formulae is presented in the appendix of Catelan (2000).

It is also worth mentioning that Soker et al. (2001) have recently suggested the possibility that stars just starting to move off the RGB toward the ZAHB location may undergo a super-wind phase, analogous to that observed in Asymptotic Giant Branch stars. This occurrence could provide a physical explanation for the gap in the HB stellar distribution at $T_{\text{eff}} \sim 20000$ K, observed in several galactic GCs.

2.3. The He-flash phase

As previously discussed, during the RGB evolution $M_{\text{core}}^{\text{He}}$ increases as a consequence of the He produced by the H-burning shell; since the core radius stays practically constant, the core density increases, and the resulting gravitational energy release raises the core temperature. In addition to this, another factor contributing to the increase of the core temperature is the steady increase with time of the temperature of the H-burning shell. The neutrino energy losses from the degenerate core also increase during the evolution. Although they do not prevent a continuous growth of the core temperature, when $M_{\text{core}}^{\text{He}}$ is larger than $\approx 0.30M_{\odot}$, they are responsible for a temperature inversion in the core, so that the temperature maximum is no longer at the stellar center but at some distance from it.

Due to the strong dependence of the 3α reaction rate on temperature, when the core gets hot enough, He-burning ignites off-center, close to the point where temperature is at its maximum. At the moment of the He-ignition in the core, density and temperature have attained values of the order of 10^6 g cm^{-3} and $8 \cdot 10^7 \text{ K}$, respectively. In electron degeneracy conditions the gas pressure does not depend on temperature, so that an expansion does not immediately follow the local temperature increase caused by the He-burning energy release. As a consequence, at first the rate of burning, not being limited by a core expansion, becomes larger and larger and a thermal runaway ensues, the so-called He-Flash (see, e.g., Iben & Renzini 1984 for a detailed discussion on the subject). However, during the He-flash, the temperature increase causes the degree of degeneracy to decrease, so that a core expansion can begin. At the same time, as the energy flux in the core increases significantly, convection sets in, efficiently carrying out the produced energy. These two factors contribute to moderate the strength of the flash so that the star is not necessarily destroyed; the efficiency of the convective energy transport is especially critical (see, e.g., Sugimoto 1964). Recent hydrodynamical simulations by Achatz (1995) and Deupree (1996) have indeed shown how the flash does not produce a hydrodynamic event. The observational evidence provided by the existence of HB stars is the best proof that the overwhelming majority of stars undergoing He-flash do not explode.

Another interesting question concerning the He-flash is the possibility of partial or total mixing between the He core and the envelope. A long time ago it has been recognized (Schwarzschild & Härm 1962, 1964, 1967, Demarque & Mengel 1972, Mengel & Gross 1976, Renzini & Fusi Pecci 1988 and references therein) that in low-mass stars such mixing does not take place, but different conclusions have been reached in the case of metal free (Pop III) or extremely metal poor stars. Fujimoto, Iben & Hollowell (1990), Hollowell, Iben & Fujimoto (1990) and Fujimoto, Ikeda & Iben (2000) found that, due to the small entropy barrier between the H- and the He-rich regions, the convective zone produced by the huge

energy release of He-burning during the He-flash can penetrate the overlying H-rich layers. The resulting inward migration of protons into high-temperature regions leads to a H-shell flash, which further increases the extension of the central convective region. At the late stages of this phase the convective envelope deepens, and merges with the convective zone. Therefore, the initially metal free surface is enriched by a large amount of matter processed via He- and H-burning reactions, in particular a very high carbon abundance follows. A deeper insight on this phenomenon is very important, since it provides an attractive working hypothesis for explaining the peculiar chemical patterns observed in extremely metal-deficient stars.

This topic has been recently addressed again by Schlattl et al. (2001, see also Weiss et al. 2000a). They have investigated in detail the evolution during the He-flash phase of metal-free stars, covering a larger parameter space with respect to the works by Fujimoto and coworkers. Schlattl et al. (2001) have confirmed earlier results pointing out that the crucial parameter which defines whether the He-flash induced mixing occurs, is the location of the point where the He-burning energy release is maximum. The deeper inside the star this point lies, the lower is the probability that the convective zone developing at the He-flash ignition can penetrate into the hydrogen-rich envelope, thereby carrying down protons and triggering a H-burning runaway.

However, even if the development of the process and its global properties are in fine agreement with the outcomes obtained by previous investigations, there is a fundamental difference: whereas Fujimoto et al. (1990) and Fujimoto et al. (2000) claim that the H-flash is a common property of all low-mass ($< 1.0M_{\odot}$) metal-deficient stars, Schlattl et al. (2001) have found that the occurrence of a H-flash critically depends on the adopted initial conditions, like stellar mass and He abundance, as well as on the inclusion and/or assumptions made for the treatment of additional physical processes like atomic diffusion

and external pollution of metals during the main sequence phase.

A preliminary comparison with some extremely metal-poor stars, such as CS22892-052 and CS22957-027 (see Schlattl et al. 2001 for details), revealed a good match of effective temperature, luminosity and the relative abundances of carbon and nitrogen, but too large absolute abundances of these elements. Even if the H-flash phenomenon provides an interesting working scenario for interpreting the observed abundance patterns in extremely metal-deficient stars, it is not yet able to provide a detailed match to the observations. Whether this occurrence is a proof of the fact that the peculiar chemical abundances observed in extremely metal-poor stars may be primordial (hence these objects are not low mass Pop III stars), due to external pollution at a late evolutionary stage, or a signature of drawbacks in current theoretical models for the He-flash phase in metal-free RGB stars, is not yet clear. ²

3. Properties of the CMD of RGB stars

The behavior of RGB models in the observational CMD follows closely their properties in the theoretical luminosity- T_{eff} diagram. We have considered, as an example, the VI (Johnson-Cousins) plane, and used the theoretical isochrones by Salaris & Weiss (1998) transformed into the VI plane according to the Alonso, Arribas & Martinez-Roger (1999) empirical color transformations³.

²Schlattl et al. (2001) have discussed some interpretations of this failure; one possibility is related to the crude assumptions made for deriving the velocity of the convective elements in the mixing region (we refer to the quoted paper for more details).

³Alonso et al. (1999) provide I magnitudes in the Johnson band. The transformation to the Cousins system has been performed following the prescriptions by Fernie (1983).

The lower panel of Fig. 2 shows the location in the $I - (V - I)$ plane of RGB isochrones of different ages and the same initial metal content, while the upper panel displays isochrones of the same age and different initial metallicities. It is evident that the RGB color at a given absolute brightness (hence the stellar T_{eff}) is very weakly affected by the age of the parent population (hence by the value of the stellar mass), at least for ages higher than a few Gyr. On the other hand, it is strongly affected by the initial value of the metallicity Z (metals mass fraction). More metal rich RGB models are redder (see upper panel of Fig. 2). This property is, from the qualitative point of view, absolutely general and does not depend on the specific color bands used, since it mirrors the behavior of the models in the luminosity- T_{eff} plane. However, the precise value of the sensitivity of RGB colors to Z does depend on the wavelength bands employed in the CMD.

Not only the color, but also the shape of the RGB is affected by Z , in a way which is strongly dependent on the wavelength bands used. This is clearly visible in the upper panel of Fig. 2, when the isochrones are plotted in the $V - (V - I)$ plane (dashed lines). In this plane the shape of the RGB is more dramatically affected, due to the behavior of the bolometric correction to the V band as a function of metallicity.

The shape and location of RGB models is almost unaffected by the selected He mass fraction Y , but it is sensitive to the metal distribution. In particular, as discussed by Salaris, Chieffi & Straniero (1993 – see also Salaris & Cassisi 1996, Salaris & Weiss 1998, Vandenberg et al. 2000), the abundance of low ionization potential elements like Mg, Si, S, Ca and Fe affects strongly the RGB temperature. In general, for typical Pop II low mass stars, RGB models computed with an arbitrary heavy element mixture will be equivalent to models with scaled solar metal ratios of the same total metallicity, as long as the ratio $\frac{X_C+X_N+X_O+X_{Ne}}{X_{Mg}+X_{Si}+X_S+X_{Ca}+X_{Fe}}$ (where X_i is the mass fraction of the element i) in the selected metal mixture is the same as in the scaled solar one. Since what is measured spectroscopically

is $[\text{Fe}/\text{H}]$ and $[\alpha/\text{Fe}]$, it is useful to consider the following relationship (Salaris et al. 1993) linking an input parameter of theoretical models like $[\text{M}/\text{H}]$ ($[\text{M}/\text{H}] \sim \log(Z/Z_\odot)$) to $[\text{Fe}/\text{H}]$ and $f_\alpha = 10^{[\alpha/\text{Fe}]}$, which holds in case of the scaled solar metal mixture by Ross-Aller (1976):

$$[\text{M}/\text{H}] \sim [\text{Fe}/\text{H}] + \log(0.638f_\alpha + 0.362) \quad (1)$$

Small adjustments to the coefficients must be applied in case of more recent determinations of the solar metal distributions; Yi et al. (2001) have obtained, in case of the Grevesse & Noels (1993) solar metal distribution:

$$[\text{M}/\text{H}] \sim [\text{Fe}/\text{H}] + \log(0.694f_\alpha + 0.306) \quad (2)$$

As far as the RGB location is concerned, this equivalence between scaled solar and α -enhanced models with the same total metallicity breaks down when Z is greater than ~ 0.002 ($[\text{M}/\text{H}] \sim -1$). In case of the TRGB and RGB bump luminosities, and the subsequent ZAHB luminosity, the previously discussed agreement between scaled solar and α -enhanced models with the same total metallicity holds for Z up to ~ 0.01 .

As for the TRGB brightness, this is weakly dependent on the stellar mass (Fig. 2), and therefore on the isochrone age, for ages larger than ~ 4 -5 Gyr. This is due to the fact that, at a given initial chemical composition, the TRGB level (and in general the stellar surface luminosity all along the RGB) is determined by the value of $M_{\text{core}}^{\text{He}}$, and its value at the He-flash is fairly constant over large part of the low-mass star range. $M_{\text{core}}^{\text{He}}$ decreases for increasing metallicity, while the TRGB brightness increases due to the increased efficiency of the H-shell, which compensates for the reduced core mass. The brightness of the subsequent ZAHB phase follows the behaviour of $M_{\text{core}}^{\text{He}}$, decreasing for increasing metallicity.

$M_{\text{I}}^{\text{TRGB}}$ appears to be also very weakly sensitive to the heavy element abundance (e.g.,

LFM93, Salaris & Cassisi 1997); for $[M/H]$ ranging between -2.0 and -0.6 , M_I^{TRGB} changes by less than 0.1 mag. In fact, $M_{\text{bol}}^{\text{TRGB}}$ is proportional⁴ to $\sim -0.18[M/H]$, while BC_I is proportional to $\sim -0.24(V - I)$ (e.g., Da Costa & Armandroff 1990). Since the color of the TRGB goes approximately as $0.57[M/H]$, then BC_I is proportional to $\sim -0.14[M/H]$. The slope of the $BC_I - [M/H]$ relationship is therefore very similar to the slope of the $M_{\text{bol}}^{\text{TRGB}} - [M/H]$ relationship, and since $M_I^{\text{TRGB}} = M_{\text{bol}}^{\text{TRGB}} - BC_I$, M_I^{TRGB} is almost independent of the stellar metal content. This is the basis for its use as distance indicator. On the other hand, due again to the behaviour of the bolometric corrections to the V band, M_V^{TRGB} is strongly affected by the metal content of the stars.

4. Properties of the LF of RGB stars

We have already defined the differential LF (or, simply, the LF) of RGB tracks (or isochrones) as the run of the number of stars per brightness bin along the RGB, as a function of the brightness itself. The number of objects in a given bin is of course determined by the local evolutionary speed, so that the comparison of observed and theoretical RGB LFs provides a key test for the accuracy of the predicted RGB timescales.

In Fig. 3 (upper panel) two V band RGB LFs (bin size of 0.1 mag), for isochrones of 13 Gyr and $Z=0.0004$ (dashed line) and $Z=0.008$ (solid line) are shown; they are normalized to the same number of stars between $M_V=2.0$ and 3.0. The local maxima located at $M_V \sim -0.2$ and 1.0 correspond to the RGB bump; the increase of the number of stars close to the TRGB of the more metal rich LF is due to the fact that the V magnitude of the RGB models at this metallicity tends to stay constant or increase slightly toward the TRGB (see Fig. 2). The overall linearity of the LF is a straightforward consequence of

⁴We are considering $[\alpha/Fe]$ ratios approximately constant with respect to $[Fe/H]$.

the existence of a luminosity - M_{core}^{He} relation (see Eggleton 1968 and Castellani, Chieffi & Norci 1989 for a detailed discussion about this point). It is evident that the ratio of the evolutionary timescales along the RGB does not depend on Z , since the slope of the LFs (i.e. the luminosity - M_{core}^{He} relation) are almost coincident.

In the lower panel of the same figure the effect of age (value of the evolving mass) is shown for two LFs with $Z=0.008$ and ages of, respectively, 10 (dotted line) and 13 (solid line) Gyr. The LF (like the CMD location) is basically unaffected by the age and only the position of the bump is slightly changed. We address the reader to the paper by Vandenberg, Larson & de Propris (1998) for a more detailed discussion about the dependence of the LF on various physical and chemical inputs.

5. RGB input physics

The quality of the agreement between observations and theory is affected by both the adequacy of the assumptions built into the stellar models, and the accuracy of the description of the physical processes accounted for. In the following, we discuss in some detail the input physics used in the current generations of RGB models, highlighting the influence on RGB stellar properties of the various choices made by different authors.

5.1. Radiative opacity

Whenever the energy is transported by radiative processes a knowledge of the radiative opacity of the stellar matter is required in order to determine the temperature gradient. Within the star, where the diffusion approximation is applied to the energy transfer equation, the Rosseland mean opacity is required. We define here as low-temperature (low- T) opacities, Rosseland mean values when $T \leq 12000$ K, and high-temperature

(high- T) opacities the values at larger temperatures. As discussed by Salaris et al (1993), it is the low- T opacities which mainly determine the T_{eff} location of theoretical RGB models, while the high- T ones enter in the determination of the mass extension of the convective envelope (through the value of the radiative temperature gradient).

Current generations of stellar models employ mainly the low- T opacity calculations by Alexander & Ferguson (1994) – and in some cases the Kurucz (1992) ones – which constitute the most up-to-date computations suitable for stellar modelling, spanning a large range of initial chemical compositions. The main difference between these two sets of data is the treatment of molecular absorption, most notably the fact that Alexander & Ferguson (1994) include the effect of the H_2O molecule. Salaris & Cassisi (1996) have compared, at different initial metallicities, stellar models produced with these two sets of opacities (as well as with the less used Neuforge 1993 ones, which provide results almost undistinguishable from models computed with Kurucz 1992 data), showing that a very good agreement exists when T_{eff} is larger than ~ 4000 K. As soon as the RGB T_{eff} goes below this limit (when the models approach the TRGB and/or their initial metallicity is increased), Alexander & Ferguson (1994) opacities produce progressively cooler models (differences reaching values of the order of 100 K or more), due to the effect of the H_2O molecule which contributes substantially to the opacity in this temperature range.

As for the high- T radiative opacities, the OPAL results (e.g. Iglesias & Rogers 1996) are generally used; these opacities, coupled with the OPAL equation of state (Rogers, Swenson & Iglesias 1996), have been repeatedly tested against helioseismological constraints (e.g., Degl’Innocenti et al. 1997), providing a good agreement between theory and observations, at least in the solar regime.

5.2. Electron conduction opacity

In the electron degenerate He-core an evaluation of the electron conduction (or, briefly, conductive) opacity is needed in order to determine the local temperature gradient. The precise computation of the conductive opacities is fundamental for deriving the correct value of the He-core mass at the He-flash, since, for example, higher conductive opacities cause a less efficient cooling of the He-core and an earlier He-ignition (i.e., at a lower core mass).

Two main choices are presently available, neither of which is totally satisfactory: the analytical fitting formulae by Itoh et al. (1983 – I83), or the old Hubbard & Lampe (1969 – HL69) tabulation. As pointed out by Catelan, de Freitas Pacheco & Horvath (1996), the most recent results by I83 are an improvement over the older HL69 ones, but their range of validity does not cover the He-cores of RGB stars. The I83 opacities are generally smaller than those obtained from the HL69 tables, thus implying larger values of M_{core}^{He} at the He-flash. Castellani & Degl’Innocenti (1999) find an increase by $0.005M_{\odot}$ of M_{core}^{He} core at the He-flash for a $0.8M_{\odot}$ model with initial metallicity $Z=0.0002$, while in case of a $1.5M_{\odot}$ star with solar chemical composition the increase amounts to $0.008M_{\odot}$ (Castellani et al. 2000). M_{core}^{He} variations of this kind imply an increase of the predicted ZAHB brightness at the RR Lyrae temperatures in the range 0.05-0.07 mag, and a slightly larger increase of the predicted TRGB brightness by ~ 0.09 mag.

It is not obvious which is the most appropriate set of opacities to use, and an extension of the I83 work to physical conditions typical of RGB cores is very much needed.

5.3. Equation of state

The equation of state (EOS) of the stellar matter is another key input for the model computations; it connects pressure, density, temperature and chemical composition at each point within the star, determines the value of the adiabatic gradient (which is the temperature gradient in most of the convective envelope), the value of the specific heat (which appears in the expression of the gravitational energy term), and plays a crucial role in the evaluation of the extension of the convective regions.

The best available EOS is probably the OPAL one (the EOS used to compute the OPAL radiative opacities), which, as already mentioned, produces remarkably good results in the solar regime. However, its range of validity does not cover either the electron degenerate cores of RGB stars, or their cooler, most external layers, below 5000 K. RGB models computed with the OPAL EOS must employ some other EOS to cover the most external and internal stellar regions. As for the models discussed later, Caloi, D’Antona & Mazzitelli (1997) and Silvestri et al. (1998) use the MHD (Däppen et al. 1988) EOS below 5000 K, while the Magni & Mazzitelli (1979) one is used for the cores; Salaris & Weiss (1998 – SW98) and Cassisi et al. (1998) complement the OPAL EOS with the Straniero (1988) one for the degenerate cores and a Saha EOS for the most external layers, while the Yale-Yonsei models (Yi et al. 2001 – YY01) employ the Yale EOS (e.g., Chaboyer & Kim 1995) for regions outside the range of validity of the OPAL data. The widely used Padova models by Girardi et al. (2000 - P00) employ their own implementation of the Straniero (1988) EOS for $T > 10^7$ K (Girardi et al 1996), and the MHD EOS at lower temperatures. Vandenberg et al. (2000 – V00) models make use of the EOS described in the appendix of their paper, while Salaris & Cassisi (1998 – SC98) RGB tracks use the EOS by Straniero (1988) throughout all the stellar structure, plus a Saha EOS below 10^6 K.

No detailed study exists highlighting the effect of the various EOS choices on the

evolution and properties of RGB stars. However, the EOS does affect the T_{eff} of stellar models in general and RGB ones in particular. After computing two $0.8M_{\odot}$ ($Z=0.001$) RGB tracks employing in the envelope either the OPAL EOS or the Straniero (1988) plus Saha one at temperatures less than 10^6 K (and keeping everything else fixed), we obtained differences of the order of more than 100 K, at least when T_{eff} is larger than about 5000 K and the envelope can be fully covered by the OPAL EOS. As far as the properties of TRGB models are concerned, a preliminary investigation on the effect of different EOS choices has been performed by Vandenberg & Irwin (1997). They have shown that neglecting the Coulomb interaction and electron exchange increases $M_{\text{core}}^{\text{He}}$ at the He-flash by $\sim 0.005M_{\odot}$ (see also Harpaz & Kovetz 1988).

5.4. Nuclear reaction rates

The He-flash in the core of RGB stars occurs when the 3α process is ignited; the rate of the 3α reactions is therefore important for determining the corresponding value of $M_{\text{core}}^{\text{He}}$. The rate by Caughlan & Fowler (1988) is widely employed; its estimated error is of about $\pm 15\%$ (see, e.g., the discussion in Castellani & Degl’Innocenti 1999), which causes a negligible uncertainty on the value of $M_{\text{core}}^{\text{He}}$ at the He-flash, of about only $\pm 0.001M_{\odot}$. If the previous rate by Fowler et al. (1975) is used, $M_{\text{core}}^{\text{He}}$ is reduced by about $0.004M_{\odot}$ (Cassisi et al. 1998).

Closely connected to the nuclear reaction rates is the evaluation of the effect of the plasma screening in stellar conditions. The screening factors usually employed are from De Witt, Graboske & Cooper (1973) and Graboske et al. (1973). The appropriate regime for the He ignition in low mass stars is the intermediate one (e.g. Graboske et al. 1973). Using the formulas for the weak screening in place of the more appropriate intermediate one causes a reduction of $M_{\text{core}}^{\text{He}}$ at the flash by $\sim 0.006M_{\odot}$ (Caloi, D’Antona & Mazzitelli 1997).

More recent developments do not modify appreciably the He-core masses obtained with this formalism (e.g. Catelan et al. 1996, Cassisi et al. 1998).

5.5. Neutrino energy losses

A precise determination of the energy losses due to neutrino emission is also important in order to determine precisely the core mass at the flash. Since neutrinos subtract energy from the stellar interior, they contribute to the cooling of the core and affect the value of core mass at He ignition (see, e.g., Sweigart & Gross 1978).

Plasma processes are the dominant mechanism for neutrino emission in the core of RGB stars; the best determination of their rate in RGB conditions is provided by Haft, Raffelt & Weiss (1994). Their formula improves the previous results by Munakata, Kohyama & Itoh (1985), which were widely used in stellar evolution calculations. Switching from the Munakata et al. (1985) results to the Haft et al. (1994) ones, produces an increase of M_{core}^{He} at the He-flash of $\sim 0.005 - 0.006 M_{\odot}$ (Haft et al. 1994, Catelan et al. 1996, Cassisi et al. 1998). The quoted uncertainty on the Haft et al. (1994) result is $\pm 5\%$, corresponding to a negligible uncertainty on the core mass at the flash (Castellani & Degl’Innocenti 1999).

A comprehensive compilation of the most recent results on the various mechanisms of neutrino emission, suitable for use in stellar evolution computations (including the Haft et al. 1994 results), can be found in Itoh et al. (1996).

5.6. Treatment of surface boundary conditions

In order to integrate the stellar structure equations it is necessary to fix the value of the pressure and temperature at the surface of the star, usually close to the photosphere.

There are basically two possibilities to do this:

i) integrating the atmospheric layers by using a $T(\tau)$ relationship, supplemented by the hydrostatic equilibrium condition and the equation of state;

ii) obtaining the desired boundary conditions from pre-computed non-gray model atmospheres.

The first procedure is universally used in the current generation of stellar models. The effects on RGB stellar models of different $T(\tau)$ relations is shown in Fig. 4, where the RGB of two 12 Gyr isochrones with $Z=0.001$ computed using, respectively, the Krishna-Swamy (1966) solar $T(\tau)$ relationship, and the gray one (see, e.g., Table 3.2 in Mihalas 1978), are displayed (all other parameters being kept fixed). RGBs computed with a gray $T(\tau)$ are systematically hotter by ~ 100 K.

Recent studies of the effect of using boundary conditions from model atmospheres are in V00 and Montalbán et al. (2001). In the same Fig. 4, as an example, we show also a RGB computed using boundary conditions from the Kurucz (1992) model atmospheres, taken at $\tau=10$. The three displayed RGBs, for consistency, have been computed by employing the same low-T opacities, namely the ones provided by Kurucz (1992), in order to be homogeneous with the model atmospheres. The model atmosphere RGB shows a slightly different slope, crossing over the evolutionary track of the models computed with the Krishna-Swamy (1966) solar $T(\tau)$, but the difference with respect to the latter stays always within $\sim \pm 50$ K. It is important to notice that the convection treatment in the adopted model atmospheres is not the same as in the underlying stellar models (i.e., a different mixing length formalism and a different value for the scale height of the convective motion is used; see next subsection for more details on the convection treatment). Montalbán et al. (2001) have discussed in detail the effect of boundary conditions from model atmospheres where convection is treated exactly as in the stellar models. Their tracks extend up to the

lower part of the RGB, where their results are qualitatively similar to ours.

5.7. Treatment of convection

The temperature gradient along the bulk of the convective envelope can be reliably approximated by the value of the adiabatic gradient; however, in the layers close to the stellar surface the convective gradient becomes strongly superadiabatic. There is no doubt that the determination of the temperature gradient in these regions is one of the most important unsolved problems of stellar evolution. The mixing length theory (MLT; Böhm-Vitense 1958) is almost universally used. It contains a number of free parameters, whose numerical values affect the model T_{eff} ; one of them is α_{MLT} , the ratio of the mixing length to the pressure scale height, which provides the scale length of the convective motions (increasing α_{MLT} increases the model T_{eff}). There exist different versions of the MLT, each one assuming different values for these parameters; however, as demonstrated by Pedersen, Vandenberg & Irwin (1990), the T_{eff} values obtained from the different formalisms can be made consistent, provided that a suitable value of α_{MLT} is selected. Therefore, at least for the evaluation of T_{eff} , the MLT is basically a one-parameter theory.

The value of α_{MLT} is usually calibrated by reproducing the solar T_{eff} , and this solar-calibrated value⁵ is then used for computing models of stars very different from the Sun (e.g. metal poor RGB and main sequence stars of various masses). It is clear that, by using the MLT, even if the input physics employed in the model computation is not accurate, it is possible to mask this shortcoming – at least from the point of view of the

⁵We notice that the solar-calibrated α_{MLT} increases by about 0.1 if element diffusion is accounted for. In the following we always refer to a α_{MLT} solar calibration without including diffusion.

predicted T_{eff} – by simply recalibrating α_{MLT} on the Sun. This guarantees that the models always predict correctly the T_{eff} of at least solar type stars. However, since the RGB location is much more sensitive to the value of α_{MLT} than the main sequence, it is important to be sure that a solar⁶ α_{MLT} is always suitable also for RGB stars of various metallicities.

Detailed 2-dimension radiation hydrodynamics simulations of stellar envelope convection spanning a large range of gravities, T_{eff} and initial chemical compositions, have been recently carried out by Ludwig, Freytag & Steffen (1999), and applied to the case of metal poor low-mass stars by Freytag & Salaris (1999). These simulations (which cover a portion of the main sequence and the lower part of the RGB), within the limit of their employed input physics and numerical accuracy, show that the T_{eff} of the Sun and RGB stars of various metallicities can be well approximated by the MLT with a constant value of α_{MLT} .

An independent way of calibrating α_{MLT} for RGB stars is to compare empirically determined RGB T_{eff} values for galactic GCs with theoretical models of the appropriate chemical composition (see also Salaris & Cassisi 1996, Vandenberg, Stetson & Bolte 1996 and references therein). In Fig. 5, as an example, we show a comparison between the T_{eff} from Frogel, Persson & Cohen (1983 – FPC83) for a sample of GCs and the α enhanced models by SW98. In principle, the distance scale plays a role, since one has to know the clusters’ distances in order to compare observed and computed RGBs; however, since the RGB is roughly vertical, uncertainties of the order of 0.2 mag in the GC distance moduli do not substantially influence the calibration. Just to give a measure of the sensitivity of the

⁶The solar calibrated numerical value of α_{MLT} depends not only on the adopted input physics, but also, as previously discussed, on the selected MLT formalism. For these reasons, to allow a comparison of the results by different authors, the adopted MLT formalism has to be specified in addition to the input physics and boundary conditions employed.

calibrated α_{MLT} value to temperature scale, chemical composition and adopted distances, we notice that systematic changes of the empirical T_{eff} by ~ 70 K, or the cluster $[\text{M}/\text{H}]$ by 0.2 dex, or the adopted cluster distance moduli by 0.25 mag, cause a variation of the calibrated α_{MLT} by ~ 0.1 . The GC reddenings have to be known to determine T_{eff} from the cluster photometry; when estimating the empirical T_{eff} with the Infrared Flux Method (IRFM), however, an uncertainty of ± 0.02 mag in the adopted GC reddening causes a variation of the calibrated α_{MLT} by less than 0.05 (e.g. Alonso et al. 2000).

Very recently Alonso et al. (2000), using the theoretical α -enhanced models by SW98, empirical estimates of T_{eff} based on the IRFM (Alonso, Arribas & Martinez Roger 1999), and the Carretta & Gratton (1997) $[\text{Fe}/\text{H}]$ scale (together with a constant $[\alpha/\text{Fe}]=0.4$ built into the theoretical models), concluded that the IRFM temperature of RGB stars in clusters spanning a wide metallicity range is adequately reproduced by theoretical models computed by adopting a mixing length value within ± 0.1 of the solar one. Also V00 found a good agreement between their solar α_{MLT} , $[\alpha/\text{Fe}]=0.3$ models and RGB T_{eff} from FPC83, for the GCs M92, M13 and 47Tuc ($[\text{Fe}/\text{H}]$ between ~ -2.3 and ~ -0.7). It is worth noting that the FPC83 temperature scale differs from the Alonso et al. (2000) one by only ~ 50 K.

These results seem to point to the fact that, as a general rule, the solar α_{MLT} value is *a priori* adequate also for RGB stars. Caution is however still necessary, for the following three main reasons. Regarding the hydrodynamical-simulations, the models reviewed before are not yet full 3D simulations, extend only up to the RGB base, and, as discussed e.g. in Zahn (1999), they are still unable to resolve all scales of convective motions. As for the calibration using empirical temperatures of RGB stars, one has to deal with the fact that it rests on the accuracy of both the T_{eff} and $[\text{Fe}/\text{H}]$ scale, together with the determination of the metal distribution. Systematic uncertainties on the GC $[\text{Fe}/\text{H}]$ scale are probably on the order of 0.2 dex (see, e.g., Rutledge, Hesser & Stetson 1997), while uncertainties on

the empirical T_{eff} scale are harder to evaluate. If color- T_{eff} relationships from theoretical model atmospheres are used to derive stellar temperatures, one has to face the associated uncertainties of the order of hundreds of Kelvin (see, e.g., Weiss & Salaris 1999). It is however important to notice that, as previously mentioned, empirical determinations based on both the IRFM (Alonso et al. 1999), or on empirical $(V - K)$ - T_{eff} relationships (FPC83), differ on average by only about 50 K.

Another source of concern about an *a priori* assumption of a solar α_{MLT} for RGB computations comes from the fact that recent models from various authors, all using a suitably calibrated solar value of α_{MLT} , do not show the same RGB temperatures. This means that – for a fixed RGB temperature scale – the calibration of α_{MLT} on the empirical T_{eff} values would not provide always the solar value. Figure 6 displays four isochrones produced by different groups (SW98, P00, V00, YY01; also the Silvestri et al. 1998 models are shown, but they will be discussed later), all computed with the same initial chemical composition, same opacities, and the appropriate solar calibrated values of α_{MLT} (we notice that the YY01 models are computed accounting for He-diffusion, and also their solar calibration of α_{MLT} is obtained considering this process). The evolving mass is the same to within $0.02M_{\odot}$, a difference which does not influence at all the RGB location. The P00 models are computed with an amount of overshooting from the formal boundary of the convective envelope, but this does not affect the RGB T_{eff} .

The V00 and SW98 models are basically identical, the P00 ones are systematically hotter by ~ 200 K, while the YY01 ones have a different shape. This comparison shows clearly that if one set of MLT solar calibrated RGBs can reproduce a set of empirical RGB temperatures, the others cannot, and therefore in some case a solar calibrated α_{MLT} value may not be adequate. The reason for these discrepancies must be due to some difference in the input physics, like the EOS and/or the boundary conditions, which is not compensated

by the solar recalibration of α_{MLT} .

To illustrate this point in more detail, Fig. 7 shows two evolutionary models for the Sun, pushed up to the RGB. The only difference between them is the treatment of the boundary conditions. Two different $T(\tau)$ relationships, namely a gray one and the Krishna-Swamy (1966) one have been employed. The value of α_{MLT} for the two models in Fig. 7 has been calibrated in each case, in order to reproduce the Sun, and in fact the two tracks completely overlap along the main sequence, but the RGBs show a difference of the order of 100 K ⁷.

This fact alone does not explain the differences among the RGBs in Fig. 6 – the P00 (and YY01) models employ a gray $T(\tau)$ while the SW98 and V00 ones a Krishna-Swamy (1966) $T(\tau)$, and the differences go in the opposite direction with respect to the effect shown in Fig. 7 – but clearly points out the fact that one cannot expect the same RGB T_{eff} from solar calibrated models not employing exactly the same input physics. The logical conclusion is that it is always necessary to compare RGB models with observations to ensure the proper calibration of α_{MLT} for RGB stars.

Before concluding this section, we recall that there exist also extensive RGB computations (Mazzitelli, D’Antona & Caloi 1995, Silvestri et al. 1998) using an alternative

⁷In this comparison the relative position of the RGBs computed with the two different $T(\tau)$ relationships is inverted with respect to the results in Fig. 4. This comes from the fact that in Fig. 4 the models were computed at constant α_{MLT} , while in Fig. 7 α_{MLT} has been recalibrated in order to match the Sun. The solar α_{MLT} obtained in case of the gray $T(\tau)$ is 1.62 (using the MLT formalism in Cox & Giuli 1968), while the Krishna-Swamy one provides 1.82; due to the higher sensitivity of the RGB to α_{MLT} , the location of the two RGBs is reversed.

formalism for the computation of the superadiabatic gradient, which in principle does not require the calibration of any free parameter. It is the so-called Full-Spectrum-Turbulence theory (FST – see, e.g., Canuto & Mazzitelli 1991, Canuto, Goldman & Mazzitelli 1996), a MLT-like formalism with a more sophisticated expression for the convective flux, and the scale-length of the convective motion fixed a priori (at each point in a convective region, it is equal to the harmonic average between the distances from the top and the bottom convective boundaries). As far as the RGB T_{eff} is concerned, the FST predicts significantly different temperatures from a solar-calibrated MLT, at least for metallicities above $Z \sim 0.001$.

In Fig. 6 an RGB computed with the FST (Silvestri et al. 1998), $Z=0.001$ and $t=12$ Gyr is also displayed. The FST computation adopted a gray $T(\tau)$ relationship as surface boundary condition, and the same opacities as the displayed MLT models. It is interesting to notice that, at least at this metallicity, the FST model is located within the temperature range spanned by the various solar calibrated α_{MLT} tracks.

Since there are basically no adjustable parameters in the FST formalism, any mismatch between predicted and observed temperatures for RGBs in GCs could still be due to systematic errors in the adopted T_{eff} and metallicity scale, and/or to inaccuracies of other aspects of the input physics, which, in case of the MLT, can be masked by a suitable calibration of α_{MLT} . It is therefore fair to say that a stringent test about the adequacy of the FST for determining the RGB T_{eff} has to wait for a final assessment of not only the RGB empirical temperature (and metallicity) scale problem, but also of all physical inputs affecting the model T_{eff} (e.g., EOS, boundary conditions).

5.8. Color transformations and bolometric corrections

As previously mentioned, one needs bolometric corrections and color transformations in order to perform comparisons between theory and observations. After a set of theoretical models is computed, there is a vast selection of available transformations that can be applied to the theoretical results; they can be divided into three categories.

i) Results from theoretical model atmospheres.

The data usually consist of tables providing bolometric corrections to the V band (BC_V), plus colors in various photometric bands, as a function of chemical composition, surface gravity and T_{eff} . These are purely theoretical results, based on the computation of large sets of model atmospheres and spectra. The latest widely available sets covering RGB models for a large range of chemical compositions are from Kurucz (1992), Buser & Kurucz (1992), Castelli, Gratton & Kurucz (1997), Castelli (1999).

ii) Results from theoretical model atmospheres, recalibrated on empirical data.

As before, but this time the theoretical colors and BC_V values have been modified (the procedure varies according to the author) in order to reproduce selected observational constraints. Examples of these transformations are the tabulations by Green (1988), Lejeune, Cuisinier & Buser (1998), Houdashelt, Bell & Sweigart (2000).

iii) Empirical transformations.

They consist of relationships between empirically determined T_{eff} , colors and BC_V at different metallicities, which are provided in term of the evolutionary phase. Alonso et al. (1996, 1999) results are the most extensive ones, covering both Main Sequence and RGB stars of spectral type F0-K5 in different photometric bands. Sekiguchi & Fukugita (2000) also have derived an empirical $(B - V)$ - T_{eff} relationship for the same class of stars. Empirical results for RGB stars are also provided by Montegriffo et al. (1998) and von Braun et

al. (1998). A severe limitation of this approach is that the range of chemical compositions and evolutionary phases covered by these transformations is strongly constrained by the evolutionary stage and chemical composition of the calibrating stars.

Due to the arbitrary zero-point of the BC_V scale (e.g., Castelli 1999), when computing V magnitudes from the values of the bolometric luminosity provided by the evolutionary tracks, and BC_V given by the selected sets of transformations, one has first to adjust the bolometric magnitude of the Sun in order to reproduce the solar visual luminosity ($M_{V,\odot}=4.82\pm 0.02$, Hayes 1985) with the provided solar BC_V (see, e.g., the discussion by Castelli 1999). An equivalent possibility is to fix the value of the bolometric magnitude of the Sun and adjust the zero point of the BC_V scale in order to reproduce $M_{V,\odot}$. With this calibration of the solar bolometric magnitude (or of the BC_V zero point) one can then consistently derive the magnitudes in other photometric bands – e.g. M_I , M_K – from the computed V magnitude and the appropriate color index, e.g. $M_I=M_V-(V-I)$, $M_K=M_V-(V-K)$. It is also worth remembering that the zero point of the color indices predicted by model atmospheres computations is usually set by reproducing the colors of Vega (e.g. Castelli 1999).

After properly calibrating the zero point of the BC_V scale, one finds that the various available sets of transformations, when applied to a given set of stellar models, provide M_V values within ~ 0.05 mag (see also Weiss & Salaris 1999). Along the RGB the derivative $\frac{\Delta color}{\Delta M_V}$ is very small, therefore this uncertainty is not particularly relevant when comparing the position of theoretical RGB models with observations. However, the same kind of uncertainty on color transformations has much more dramatic consequences.

Let us consider, as an example, the $V - (V - I)$ Johnson-Cousins CMD (the situation in other photometric bands is similar, if not worse). Figure 8 displays an isochrone with $Z=0.001$ and $t=10$ Gyr (from Salaris & Weiss 1998) using 4 different sets of transformations,

namely, the ATLAS 9 theoretical transformations from Castelli, Gratton & Kurucz (1997), the semiempirical ones by Green (1988) and Lejeune et al. (1998), and the empirical ones by Alonso et al. (1999), based on the IRFM temperature scale. For the sake of comparison, filled circles and empty squares denote the RGB location of Galactic GCs with this metallicity (assuming the same $[\alpha/\text{Fe}]$ enhancement as in the Salaris & Weiss 1998 models), taken from the analytical relationships by Saviane et al. (2000) for the HB distance scale by Lee, Demarque & Zinn (1990 – choices of the distance scale differing by $\sim \pm 0.10$ mag around this value do not appreciably modify the comparison) and, respectively, the Carretta & Gratton (1997) $[\text{Fe}/\text{H}]$ scale (filled circles) and the Zinn & West (1984) one (empty squares).

The differences in the RGB location and shape of the theoretical models are basically due to the differences in the color- T_{eff} relationships. At a fixed value of M_V , $(V - I)$ color differences span a range between ~ 0.05 and ~ 0.10 magnitudes. This range of colors implies an uncertainty of $\sim 0.3 - 0.5$ dex when determining $[\text{Fe}/\text{H}]$ from the comparison of observed and theoretical RGB CMDs. If the color difference between Turn-Off (TO) and base of the RGB is employed to estimate GC absolute ages, the uncertainty on the derived age would be again very high (assuming the main sequence color is unchanged), since a variation by $\sim 0.01 - 0.02$ mag of this color difference corresponds to an age variation by about 1 Gyr.

6. The CMD as a tool for calibrating RGB models

A comparison between the observed and predicted CMD location of RGB models allows one in principle to test the reliability of the physical inputs employed to compute the structure of the stellar external layers. This is because, as previously discussed, the CMD location of RGB stars depends on the description of the envelope superadiabatic region (low-T opacities and convection treatment), the envelope EOS, the surface boundary

conditions and color transformations adopted.

Da Costa & Armandroff (1990) and more recently Saviane et al. (2000) and Ferraro et al. (2000) have published very useful relationships between colors and morphology of the RGB as a function of $[\text{Fe}/\text{H}]$, from multicolor observations of a sample of galactic GCs. These relationships provide a test-bench for theoretical models, even though they depend on the adopted $[\text{Fe}/\text{H}]$ scale (still somewhat uncertain, as already mentioned), cluster reddenings and, to a lesser extent, on the assumed distance scale. The general trends with respect to the stellar metallicity (change of location and shape of the RGB, and their dependence on the wavelength bands employed) predicted by the models are in broad qualitative agreement with observations, but the empirical relationships are more easily used to calibrate the RGB models rather than testing their reliability. Because of the still relevant uncertainties in the predicted CMD location of RGB models – compare, e.g., the range of shapes, T_{eff} and colors attainable by selecting various combinations of the different theoretical models and color transformations displayed in Figs. 6 and 8 – a comparison of theory with observations can be used to calibrate the mixing length and constrain the color transformations adopted in the model computations. This is precisely the approach followed by, e.g., Weiss & Salaris (1999) and V00.

7. Surface abundances and mixing mechanisms along the RGB

The standard notion of element abundance variations in GC stars is that, within the errors, there are no intra-cluster variations. To first order, and with only a small number of exceptions (ω Cen, and possibly M22), this seems to be correct. Looking at detailed individual abundances, however, this is no longer true. As a consequence of the first dredge-up, standard RGB models predict a modest change in elements participating in proton-capture nucleosynthesis (§ 2.1). Since the depth of convective mixing extends to

layers with $T \approx 2 \cdot 10^6$ K at most, only helium, lithium, carbon and nitrogen and their isotopes are concerned. In particular, the $^{12}\text{C}/^{13}\text{C}$ ratio is predicted to drop from the initial cosmic value of 90 to about 25, but not to that of CN-equilibrium, which is of order 3. These variations are predicted to take place near the base of the RGB in low- and intermediate mass stars, and agree with observations.

This canonical picture about RGB abundances, however, is challenged by an increasing amount of observational data demonstrating its limited validity. In the following, we will summarize this observational material and discuss possible theoretical explanations. In the context of this review, these observations clearly demonstrate that the physical processes taken into account in canonical stellar evolution calculations are insufficient and that the theory needs to be extended. The reader may find additional material in the excellent reviews by Kraft (1994) and Da Costa (1998), although the amount of observations has grown a lot since their publication.

7.1. The observational evidence

7.1.1. Metal-poor field stars

There is now large evidence for mixing beyond the canonical first dredge-up prediction in metal-poor field stars. Charbonnel & do Nascimento (1998) summarized the literature data to find that in 95% of the low-mass metal-poor field stars the $^{12}\text{C}/^{13}\text{C}$ ratio is lower than expected. The average value is of order 10, but a few stars also reach $^{12}\text{C}/^{13}\text{C} \leq 6$. Charbonnel & do Nascimento (1998) identify two interesting trends: firstly, there is a clear anti-correlation between isotope ratio and brightness, setting in at $M_V < 2$, i.e. approximately at the level of the RGB bump, and secondly, the lowest $^{12}\text{C}/^{13}\text{C}$ values are reached by those stars showing the highest surface rotation, $v \sin i$. The first fact provides

substantial evidence that the isotope anomaly is due to intrinsic extra-mixing beyond the established first dredge-up during RGB evolution; the second one hints that there is a correlation with rotation, which might possibly initiate this additional mixing.

Gratton et al. (2000) confirmed these results by a dedicated abundance analysis of 62 low-mass metal-poor field stars with HIPPARCOS parallaxes. They confirmed the trends found earlier and added additional details. They conclude that a second mixing episode sets in after the bump, resulting in lowered carbon abundances and carbon isotope ratios (but “distinctly higher than the equilibrium value”), an increased nitrogen and a declining Li abundance down to almost zero. They confirm that this happens in basically all stars of their own sample and 43 additional stars from the literature. The anticorrelation with brightness is evident, too. Another very important result is that neither O nor Na show any abundance variation in these field stars. This is, as we shall see below, quite different from similar stars in globular clusters.

Most recently, Keller, Pilachowski & Sneden (2001) confirmed the carbon isotope results from IR-data. From a sample of literature data they also find that the amount of mixing seems to decline with increasing metallicity.

7.1.2. Globular cluster stars

The quantity and quality of observations and the rate of new data acquisition is impressive. In the following, only a few highlights illustrating the main trends can be mentioned. For more extended references to observational material the reader should consult the current literature.

Carbon abundance variations along GC RGBs have been detected as early as 1979 in M92 (Bell, Dickens & Gustafsson 1979), the cluster which remains to be one of the most

important cases displaying evolutionary effects (Carbon et al. 1982, Langer et al. 1986, Bellman et al. 2001). The variations are in agreement with those in field stars, i.e. a declining carbon abundance and isotope ratio, and an increasing nitrogen abundance with brightness. Similar cases include M15 (Trefzger et al. 1983), NGC 6397 (Briley et al. 1990). In addition, star-to-star variations in O and Na were detected in a significant number of clusters, most prominently in NGC 6752 (Suntzeff & Smith 1991), NGC 3201 (Gonzalez & Wallerstein 1998), M3 (Suntzeff 1981) and M13 (Suntzeff 1981, Pilachowski et al. 1996), the latter cluster exhibiting the most extreme spread in abundances. ω Cen (Norris & Da Costa 1995), the only cluster with a clear intra-cluster iron abundance (or total metallicity) spread, also displays the full spectrum of anomalies. Oxygen tends to be underabundant by up to 0.5 to 1.0 dex with respect to the standard, α -enhanced metal composition ($[\text{O}/\text{Fe}] \sim 0.4$), while sodium is overabundant up to more than 0.5 dex. The important point is that the two elements are anticorrelated in their abundance variations. There is – in contrast to the CNO-elements – no clear evidence for a development of the anomalies along the RGB, although in M13 they seem to be absent below the bump, but fully developed above it. Most importantly, and as mentioned above, the O-Na-anticorrelation or any other anomaly in their abundances is definitely absent in field stars (Gratton et al. 2000). This points to the influence of some environmental effect.

Many of the best observations have been obtained with the KECK/HIRES instrument, although smaller telescopes are sufficient for spectroscopy of the brightest stars. Since the year 2000, the VLT/UVES instrument has become available, allowing the observations of cluster stars at the subgiant branch (SGB) or TO. First results have been published already by Castilho et al. (2000) and Gratton et al. (2001) about NGC 6397 and NGC 6752. While for the first cluster the comparison between TO- and SGB-stars shows no significant abundance differences and a very low scatter in oxygen, NGC 6752 already displays the full range of the O-Na-anticorrelation close to the main sequence. These observations provide

strong evidence for a non-evolutionary source for the abundance anomalies, as do the results by King et al. (1998) about M92, in which the corresponding Na and Mg (see below) anomalies are claimed to be found in subgiants, too.

More metal-rich clusters ($[\text{Fe}/\text{H}] \geq -1.4$) support this: in a number of clusters (47 Tuc, Cannon et al. 1998; M4, Ivans et al. 1999; M71, Briley & Cohen 2001) a bimodal C-N abundance distribution is present all along the cluster sequence, or – as in M5 (Ivans et al. 2001) – the extent of the anomaly may even be anti-correlated with evolutionary state. All these facts are interpreted in terms of the presence of a primordial source such as contamination by more massive stars.

The final point in favor of a primordial component responsible for at least some abundance variations is the fact that also a Mg-Al-anticorrelation has been found in several clusters (among them ω Cen, Norris & Da Costa 1995; M13, Shetrone 1996a; M4, Ivans et al. 1999), where Al can be overabundant by up to 1 dex. As will be discussed below, the conversion of ^{24}Mg to ^{27}Al is possible only in stars more evolved than the RGB, since temperatures of $\approx 7 \cdot 10^7\text{K}$ are needed (Langer, Hoffman & Zaidins 1997). Al-production from other Mg-isotopes fails to explain the high Al-enrichment and leads to conflicts with the Na-abundance trends. The high Al abundances found in cluster stars are probably the most difficult anomaly to be explained.

7.2. Proton-capture nucleosynthesis

The result of the standard first dredge-up, taking place on the SGB and lower RGB is to transport material that has participated in hydrogen-burning into the convective envelope, mixing it there with matter of the initial composition. The observed abundances of CNO-elements are in complete agreement with the theoretical predictions, and in

particular show the constancy of the sum of C, N, and O, the proper correlations, and isotope ratios. They can be explained, thus, by mixing of proton-capture nucleosynthesis products.

In addition to the well-known CNO-cycle, analogous reaction cycles involving heavier elements exist at higher temperature. In Fig. 9 we show the NeNa- and MgAl-cycles and in Fig. 10 the abundance profiles in and above the hydrogen-burning shell of a typical RGB cluster star. It is obvious that abundance variations due to first proton-capture reactions, such as the C→N conversion appear outside the region of a significantly reduced H-abundance and thus of a varying molecular weight.

The elements affected (C, N, O, Ne, Na, Mg, Al) are exactly those which show star-to-star variations in clusters, providing the first evidence that the anomalies are the result of proton-capture reactions. Denissenkov & Denissenkova (1990) demonstrated that the O-Na-anticorrelation can be explained self-consistently by the assumption that both elements have been subject to nuclear processing in a typical RGB hydrogen-shell. The crucial point is that Na and O are not participating in the same cycle (as is the case for the C-N-anticorrelation), but in the NeNa- and CNO-cycle, respectively. However, within the shell oxygen is depleted and sodium enhanced at the same location, and hence temperature (see Fig. 10; the first rise at $0.08 \lesssim \delta m \lesssim 0.13$ of the model shown). Note that in the outermost layers of this region Na is enhanced without significant depletion of O; such cases are observed, too. Unfortunately, the accompanying Ne-depletion cannot be detected. Langer, Hoffman & Sneden (1993) and others confirmed that a typical RGB H-shell could be the source for the anomalies up to Na, and since then the observations are being explained in terms of proton-capture nucleosynthesis. The most up-to-date reaction rates as well as a discussion of their errors can be found in Arnould, Goriely & Jorissen (1999).

It is of special interest that the stable aluminium isotope ^{27}Al is produced only in

the very deep interior of the H-shell and at the expense of ^{25}Mg (Fig. 10, where the initial magnesium abundance was raised to $[^{25}\text{Mg}/\text{Fe}] = 1.2$; see below). Langer & Hoffman (1995) investigated in detail the nucleosynthesis of Na, Al and Mg. Their results can be summarized as follows: (i) under RGB-typical conditions Al is produced almost exclusively at the expense of ^{25}Mg ; for isotope and element ratios typical of field halo stars this results in only a modest Al enrichment of ≈ 0.3 dex; (ii) to reach the high $[\text{Al}/\text{Fe}]$ -levels observed, $[^{25}\text{Mg}/\text{Fe}] \gtrsim 1.0$ has to be assumed; (iii) the conversion of ^{25}Mg into ^{27}Al leads to a depletion of only 0.2 dex in Mg; (iv) significant Al-production happens only at very high temperatures; as a consequence, helium-enriched material is mixed into the envelope. The second of these points requires an additional primordial component and the first one is in contradiction with the fact that it is ^{24}Mg , which is depleted in M13 (Shetrone 1996b, but see Ivans et al. 1999 for a different result on M4). And finally, the depletion of Mg in M13 is as large as 0.4 dex, which can be reconciled with (iii) only with difficulties. A further complication arises from the fact that nucleosynthesis calculations show that Na has a higher overproduction than Al (Langer et al. 1993), while observations (Norris & Da Costa 1995) indicate the opposite. Langer et al. (1997) showed that a better agreement with all element abundances can be reached if the burning temperature of the hydrogen shell is assumed to be around $7 \cdot 10^7$ K, more typical for asymptotic giant branch (AGB) stars. In RGB stars, $5.5 \cdot 10^7$ K is the maximum value reached by very metal-poor stars close to TRGB, while Al is overabundant at much lower brightness as well.

7.3. Theoretical models for the abundance anomalies

7.3.1. Evolutionary scenario

The very clear evidence from field stars (§ 7.1.1) and CN-variations in some clusters (§ 7.1.2) requires that at least part of the complete explanation for all the anomalies

discussed is to be found in a non-canonical effect taking place during the RGB-phase, due to which the products of nucleosynthesis in the red giant’s own H-burning shell appear at the surface. This requires some additional mixing between shell and the bottom of the convective envelope. The mixing must be rather slow, otherwise the trends with luminosity would not be observed and the whole envelope could probably be processed by the shell. Most of the observations supporting this evolutionary scenario indicate that the extra mixing sets in at or after the bump, i.e. the point at which there is an almost vanishing difference in molecular weight between the outer shell regions ($\delta m \gtrsim 0.10$ in Fig. 10) and the convective envelope. However, in M92 the carbon depletion might start even earlier than that (see Bellman et al. 2001).

Evolutionary models, pioneered by Sweigart & Mengel (1979), therefore try to reproduce the observations by adding proton-capture nucleosynthesis in the NeNa- and MgAl-cycles and some kind of extra-mixing to the canonical stellar evolution calculations. Different implementations ranging from ‘conveyor belt’ approaches (Wasserburg, Boothroyd & Sackmann 1995) to models fully incorporating diffusive mixing (Charbonnel 1995, Weiss, Denissenkov & Charbonnel 2000b) exist, but none is – up to the present time – completely self-consistent, in the sense that the physical reason for the mixing (probably differential rotation), its extent and speed, the full nucleosynthesis, and the back-reaction on the model are solved simultaneously. In the following we will describe a two-stage approach used by Denissenkov & Weiss (Denissenkov & Weiss 1996, and later work) and – in a slightly variant form – by Cavallo, Sweigart & Bell (1998, and follow-up work).

This method separates the canonical from the non-canonical aspects of the problem. A stellar model of appropriate mass (typically $0.8 M_{\odot}$) and composition is evolved within the canonical framework along the RGB. Several models at various epochs are then used for the background structure ($M_r(r)$, $T(r)$, $P(r)$, $L_r(r)$) on which the extra-mixing and

detailed nucleosynthesis are performed. The background structure of the region between shell and convective envelope can be obtained for any given timestep by interpolation in the relative coordinate $\delta m = (m_r - m_{bs}) / (m_{bcz} - m_{bs})$, where m_{bs} and m_{bcz} are the relative mass coordinates of the bottom of shell and convective zone, respectively (Denissenkov & Weiss 1996). Nucleosynthesis then is calculated with this background physical structure, by using an extensive network of up to 26 nuclei and 69 reactions (Denissenkov et al. 1998). The mixing is done by solving a diffusion equation with diffusive speed (the diffusion constant) and penetration depth as free parameters. Both are identical for all elements. The advantage of such an approach is that it allows the calculation of a range of extra-mixing parameters and an economical exploration of stellar metallicity (Cavallo et al. 1998). The disadvantage is that it has to assume that the mixing has no influence on the background structure evolution, i.e. that there is no significant back-reaction. Obviously, the approach is always inconsistent as the mixing of the various metals has not been taken into account in the stellar model calculations. As long as no change in the H/He-profile takes place and thus the mixing does not touch regions of declining hydrogen abundance in the shell ($\delta m \lesssim 0.08$), the hope is that the inconsistency does not pose a severe problem. However, it also implies that no very deep mixing can be investigated.

All results confirm that CN- and ONa-abundance anomalies can be reproduced by the deep-mixing scenario with reasonable mixing assumptions (e.g., Langer et al. 1993, Charbonnel 1995, Denissenkov & Weiss 1996, Cavallo et al. 1998, Denissenkov & Tout 2001). In a number of papers, these assumptions are based on a physical model for rotation-induced mixing. For example, the results by Denissenkov & Tout (2001), repeated in Fig. 11, were obtained this way. Due to the physical approach the derived effective diffusion constant varies with depth, and is of order $10^8 - 10^9 \text{ cm}^2 \text{ s}^{-1}$. The diffusive speed drops toward zero at $\delta m \approx 0.08$; this point corresponds to the mixing depth used in Denissenkov & Weiss (1996) and Weiss et al. (2000b). These numbers are in good agreement with the parameters used

in the two papers quoted. The penetration depths are actually shallow enough to justify the two-stage approach. Figs. 11 and 12 illustrate the successful reproduction of observed anomalies in several clusters.

As a (rather important) side-effect, the additional mixing also ensures that most of ${}^3\text{He}$ produced in the pp-I-chain on the main-sequence is destroyed, thereby resolving one of the problems of galactic chemical evolution – that of ${}^3\text{He}$ -overproduction (see Charbonnel & do Nascimento 1998, Weiss et al. 1996, and references therein).

The calculations based on rotation-induced mixing (Charbonnel 1995, Denissenkov & Tout 2001) also predict that the mixing is not able to penetrate significant molecular weight changes (Charbonnel, Brown & Wallerstein 1998), supporting the picture that the evolutionary effects can start only at or after the bump and that no significant amounts of helium will be mixed to the surface. The same models predict that no additional mixing takes place in stars of $M \gtrsim 2.0 M_{\odot}$ and that the degree of extra-mixing diminishes with increasing metallicity (Cavallo et al. 1998). This is in agreement with observations (e.g. Gilroy 1989 and Briley, Smith & Claver 2001).

In contrast to this, Sweigart(1997a,b), argued for a penetration of the molecular weight barrier and resulting helium mixing accompanying extreme O-Na-anomalies such as those found in M13. Such ‘very deep mixing’ would have significant bearing for both the evolution along the RGB, the brightness of the TRGB, the HB brightness level and the HB morphology. Some of these predictions will be discussed further in § 8 and § 9.1. Weiss et al. (2000b) investigated the consequences on the proton-capture element abundances with models in which the helium mixing itself was included into the full stellar evolution calculations (to account for the structural changes) and concluded that noticeable helium mixing would be accompanied by extreme O and Na changes (resulting from the second Na rise in Fig. 10) exceeding the observed levels. Therefore, based purely on nucleosynthesis

arguments, the mixing of regions with $\Delta X \gtrsim 0.1$ could be excluded; on the other hand, Weiss et al. (2000b) also found models which evolved to very high luminosities without strong helium mixing into the envelope and without violating the abundance observations. However, these were preliminary results to be investigated further with more physical mixing models.

The ‘normal deep mixing’ models all fail to explain the Mg-Al anticorrelation, because of the temperatures in the shell regions affected by the deep mixing being too low for Al production from ^{24}Mg . Fujimoto, Aikawa & Kato (1999), and Aikawa, Fujimoto & Kato (2001) proposed a variant of the deep mixing scenario, where the mixing repeatedly penetrates the whole H-shell, mixing protons into the hot helium-core, leading to shell flashes, in which also Al is synthesized. This scenario is in fact very similar to the helium-flash in Pop III stars discussed in § 2.3. While this model succeeds in reproducing several abundance trends, which remain unexplained in the simple deep-mixing scenario, the models are simple box-models (i.e. no complete stellar models) so far, and a physical explanation for these extreme mixing events is even more difficult.

Concerning the Al problem, Langer & Hoffman (1995) noted that significant amounts of the radioactively unstable isotope ^{26}Al (lifetime: $\approx 10^6$ years) can be produced in the same shell regions which are responsible for the O-Na-anticorrelation. Denissenkov & Weiss (2001) investigated this in detail with the two-stage method and demonstrated that under the assumption that the observed Al is actually ^{26}Al , all known correlations in ω Cen and M4 (Fig. 12) can be simultaneously explained with standard mixing parameters. In fact, the mixing speed is high enough as compared to the isotope’s lifetime that enough ^{26}Al is always transported to the surface, replacing the decayed atoms. If the Al could be confirmed as ^{26}Al , either by isotopic line shifts or the emitted 1.8 MeV γ -line (both not being possible as yet), this would be a direct proof for the on-going mixing process. As

mentioned earlier, these models also needed a primordial enrichment of ^{25}Mg by a factor 10.

7.3.2. *Primordial scenarios*

As was shown in § 7.1.2 and § 7.2 there are a number of arguments in favor of a primordial component: These are the failure to produce the large Al-overabundances in standard RGB H-shells consistently with the Mg and Na data, and the finding of anomalies in a number of cluster stars already on the SGB, or even earlier. Also, Ivans et al. (1999) argue that in M4 there exists a “primordial floor” of abundance anomalies (notably in Al), on which an evolutionary component is superimposed.

Most papers employing primordial components turn to AGB-stars of higher mass, in which proton-nucleosynthesis takes place at higher temperatures. We refer the reader to Denissenkov, Weiss & Wagenhuber (1997), Denissenkov et al. (1998) and Ventura et al. (2001); the latter is focused on the so-called hot-bottom burning phase. This approach explains in particular the high Al and low Mg (probably ^{24}Mg) observed in two subgiants in NGC 6752 (Gratton et al. 2001). Since in the primordial picture the nucleosynthesis and mass loss takes place in more advanced stages of evolution, we will not go into the details here.

7.4. **Summary of RGB abundance anomalies and consequences**

The existence of star-to-star variations in the abundances of proton-capture elements has been demonstrated without doubt. In fact, it appears as if they are a generic property of all low-mass ($M \lesssim 2.0 M_{\odot}$) metal-poor stars, as long as they are restricted to CNO-elements. The same data strongly point to an intrinsic evolutionary process in red giants, which still has to be fully understood and incorporated into self-consistent models.

Only cluster stars seem to exhibit the anomalies in heavier elements (Na, O, Mg, Al) as well. It is not yet clear, whether an evolutionary component is necessary to explain those, but a primordial one seems unavoidable. This will lead to interesting consequences for the intra-cluster gas chemical evolution.

Although some reactions in the NeNa- and MgAl-cycles are still uncertain, this general picture will not depend on them. However, nuclear data would be of great help to narrow the range of conditions for proton-capture nucleosynthesis. And finally, abundance data as a function of luminosity along cluster sequences are necessary from the TO to the TRGB in order to investigate the contributions of primordial and evolutionary components.

Before concluding this section, we notice that, as long as one tries to explain by deep mixing only the CNO and NeNa-cycle anomalies, and therefore no appreciable amount of hydrogen is brought into the shell (and helium dredged into the envelope), the evolutionary timescales and RGB location predicted by canonical models are not affected by this added element transport mechanism (see, e.g., Weiss et al. 2000b and discussion in §8).

8. The LF as a tool for testing the inner structure of RGB models

The analysis of the RGB LF is of paramount importance in order to check the accuracy of the inner structure of theoretical RGB models. In particular, as discussed by Renzini & Fusi-Pecci (1988), through the LF one can test the chemical stratification inside the star. This follows from the fact that the hydrogen abundance sampled by the thin H-burning shell strongly affects the rate of evolution, hence the star counts along the RGB. When a statistically sizeable sample of RGB stars is available, one could expect to check the envelope chemical profile with a mass resolution of the same order of magnitude of the shell thickness. Moreover, the LF is unaffected by the existing uncertainties in the T_{eff} and color

determination.

Langer, Bolte & Sandquist (2000) have recently claimed the existence of a discrepancy between the theoretical and observed RGB LF of the two GCs, M5 and M30 (see also Vandenberg et al. 1998) . They found an overabundance on stars in the upper RGB, arguing that the cause might be the action of some very deep mixing mechanism active during the RGB ascent. This deep mixing (see §7 for a more detailed discussion about this point) would be able to bring some hydrogen from the envelope into the H-burning shell (and therefore an extra amount of He in the envelope), causing a longer lifetime and an increase of the number of observed RGB stars. A recent analysis by Zoccali & Piotto (2000) has found however a good general agreement between various sets of theoretical LFs and observations of a large sample of GCs – some of which show the abundance anomalies discussed in §7 –, at least below $[\text{Fe}/\text{H}] \sim -0.7$. Possible discrepancies at higher metallicity, in the upper part of the RGB, need to be confirmed with further observational data. The LF slope predicted by theoretical models and its independence of the initial stellar metallicity looks therefore confirmed, supporting the relative timescale along the RGB predicted by canonical models, and showing that deep mixing, if effective, does not appreciably affect the predictions of canonical RGB models. A similar conclusion has been reached by Rood et al. (1999) in their study of the LF of M3.

8.1. The RGB bump brightness

As already mentioned, during the RGB evolution the H-burning shell crosses the chemical discontinuity left over by the convective envelope soon after the first dredge-up. When the shell encounters this discontinuity, matter in the shell expands and cools slightly, causing a sharp drop in the stellar surface luminosity. After a while, thermal equilibrium is achieved again and the stellar luminosity starts to monotonically increase up to the TRGB.

As a consequence, the structure passes three times across a narrow magnitude interval. This occurrence produces the characteristic bump in the theoretical LF.

Since its detection in 47Tuc, the RGB bump has become the crossroad of several theoretical and observational investigations (Fusi Pecci et al. 1990, Alves & Sarajedini 1999, Ferraro et al. 1999, Zoccali et al. 1999). In order to detect the bump a large sample of RGB stars is required – $\sim 10^3$ stars in the upper four magnitudes of the RGB according to Fusi Pecci et al. (1990) – and until a few years ago it was detected only in metal-rich stars. In fact, increasing the cluster metallicity, the luminosity extension of the bump is larger and it is also shifted to lower luminosity, in a more populated RGB portion; both effects work in the direction of making the bump detection easier. Only in this last decade, thanks to the HST capability of imaging the dense GC cores, and the availability of large field CCD detectors, has the RGB bump been detected also in metal-poor GCs.

Since the position of the bump is related to the location inside the stellar structure of the H-discontinuity, the deeper the chemical discontinuity is located, the fainter the bump luminosity will be. A comparison of the theoretical bump level with observations allows a test of the predicted maximum extension of the convective envelope in RGB models. The parameter $\Delta V_{\text{HB}}^{\text{Bump}} = V_{\text{Bump}} - V_{\text{HB}}$ – the V-magnitude difference between the RGB bump and the HB at the RR Lyrae instability strip level (Fusi Pecci et al. 1990, Cassisi & Salaris 1997, hereinafter CS97) – is commonly adopted as a measure of the bump brightness. From the observational point of view it is a distance independent quantity, but theoretically $\Delta V_{\text{HB}}^{\text{Bump}}$ depends not only on the bump level predicted by models, but also on the HB luminosity set by the value of $M_{\text{core}}^{\text{He}}$ at the He-flash, which is still subject to the uncertainties discussed before.

For a given set of input physics employed in the model computation $\Delta V_{\text{HB}}^{\text{Bump}}$ is affected mainly by the total metallicity [M/H] and the age of the cluster. As far as the age is

concerned, an increase by 1 Gyr at a given metallicity causes an increase of $\Delta V_{\text{HB}}^{\text{Bump}}$ by about 0.024 mag. As the HB luminosity is almost unaffected by the age – for typical GC ages – this change is due to the change in the bump luminosity: when the cluster age increases, the mass of the evolving RGB star decreases, and the H-discontinuity location deepens because of the larger convective regions. The effect associated with the cluster metallicity is significantly more relevant. For an age of 15 Gyr, a change by +0.20 dex of $[M/H]$ increases $\Delta V_{\text{HB}}^{\text{Bump}}$ by $\sim 0.1 - 0.2$ mag (the precise value depending on the actual metallicity). This is a consequence of the fact that the larger the star metallicity, the larger is the mass extension of the convective envelopes (larger radiative opacities within the structure) and the dimmer is the bump level; at the same time, when the metallicity increases, the HB becomes fainter because of the smaller $M_{\text{core}}^{\text{He}}$ at the He-flash, but this brightness decrease is smaller than the change of the bump level, so that $\Delta V_{\text{HB}}^{\text{Bump}}$ increases.

As a reference, we provide here the relationship derived from the canonical models by CS97, for a cluster age equal to 15 Gyr and in the whole Galactic GCs metallicity range:

$$\Delta V_{\text{HB}}^{\text{Bump}} = 1.083 + 1.380[M/H] + 0.231[M/H]^2 \quad (3)$$

The first exhaustive comparison between theory and observations of $\Delta V_{\text{HB}}^{\text{Bump}}$ in galactic GCs has been performed by Fusi Pecci et al. (1990). Using the theoretical models available at that time, they found that the observed dependence of $\Delta V_{\text{HB}}^{\text{Bump}}$ on cluster metallicity is in good agreement with theoretical predictions, but theoretical $\Delta V_{\text{HB}}^{\text{Bump}}$ values were smaller than the observed ones by ≈ 0.4 mag. For a long time, this result has been considered a clear drawback of canonical theoretical models of low-mass RGB stars. It was therefore suggested by Alongi et al. (1991) that this discrepancy can be removed accounting for the efficiency of overshooting from the base of the formal boundary of the convective envelope, which shifts the bump level to a lower brightness, because of the resulting deeper convective

envelope. By parametrizing the mass extension of the overshooting region in units of the local pressure scale height (H_p), it was shown that an overshooting region of $\sim 0.7H_p$ could resolve the discrepancy.

More recently, CS97 have reanalyzed the problem using their updated canonical stellar models applied to a sample of 8 clusters with spectroscopical determinations of $[\text{Fe}/\text{H}]$ and $[\alpha/\text{Fe}]$, taking explicitly into account the effect of the α -element overabundance. They concluded that their models (see previous relationship) provide a good match to observations. Zoccali et al. (1999) and Ferraro et al. (1999) have later produced observational $\Delta V_{\text{HB}}^{\text{Bump}}$ databases for, respectively, 28 clusters obtained from HST observations – all calibrated and reduced homogeneously – and 40 clusters taken from literature data. In Fig. 13 (top panel), we show the comparison between models by CS97 and the Zoccali et al. (1999) data, plus additional clusters from the Ferraro et al. (1999) catalogue. We have adopted the $[\text{Fe}/\text{H}]$ scale provided by Carretta & Gratton (1997) and the labeled assumptions about the trend of the α -element enhancement with the iron abundances (see Zoccali et al. 1999 for a full discussion). We have considered an uncertainty on the global metallicity $[\text{M}/\text{H}]$ of the order of 0.15 dex, which perhaps is a lower limit for the true uncertainties affecting both $[\text{Fe}/\text{H}]$ and $[\alpha/\text{Fe}]$ measurements (Carney 1996, Rutledge, Hesser & Stetson 1997).

The top panel of Fig. 13 shows a good agreement between theory and observations. In order to account for the current uncertainty on the zero point of the GC $[\text{Fe}/\text{H}]$ scale, the bottom panel shows the same comparison employing the Zinn & West (1984) $[\text{Fe}/\text{H}]$ scale. In this case, the agreement between theory and observations is worse, at least for metallicity lower than $[\text{M}/\text{H}] < -1.0$, where the two $[\text{Fe}/\text{H}]$ scales are most different: the disagreement with theoretical predictions for a cluster age of 14 Gyrs is on average of about 0.20 mag, a value which is almost a factor of 2 larger than the mean photometric uncertainty.

Bergbusch & Vandenberg (2001) found a discrepancy of about 0.25 mag when comparing the results from their isochrones (V00 models) with $\Delta V_{\text{HB}}^{\text{Bump}}$ data for 4 GCs at various metallicities (see their Figure 17). The bump brightness from their models is in good agreement with the CS97 results, while their HB models are about 0.05 mag fainter; the GC [Fe/H] values adopted in their comparison are within 0.1 dex of those by Zinn & West (1984), whose metallicity scale they favored from other considerations.

The conclusion to draw from this discussion is that the discrepancy found by Fusi Pecci et al. (1990) may well be reduced to zero without the need to include overshooting, but lingering uncertainties on the HB theoretical brightness (due to the already discussed uncertainties on the $M_{\text{core}}^{\text{He}}$ value at the He-flash) and GC metallicity scale, leaves open the possibility that a discrepancy at the level of ~ 0.20 mag between theory and observations may still exist, and one possibility to solve this discrepancy, if real, would be to consider overshooting from the convective envelope, as in the P00 models.

8.2. Stellar counts across the RGB Bump.

The brightness of the LF bump is a diagnostic of the maximum extension of the convective envelope reached at the base of the RGB, but it does not provide information on the size of the jump in the H profile left over when the envelope starts to recede. Since the evolutionary rate along the RGB is strongly affected by any change in the chemical profile, it is clear that this information can be obtained by analyzing the star counts in the bump region. This is a further test for the accuracy and adequacy of canonical RGB models which has been performed by Bono et al. (2001). They have defined a new parameter – R_{bump} – which is the ratio between the number of stars in the region within $V_{\text{bump}} \pm 0.4$ mag and the number of RGB stars in the interval $V_{\text{bump}} + 0.5 < V < V_{\text{bump}} - 0.5$, (where V_{bump} is the central magnitude of the bump region) and compared theory with observation for a large

sample of GCs, using the theoretical models by CS97.

Figure 14 shows this comparison, and displays also the small dependence of R_{bump} on age and initial He content. It is also evident that the selected $[\text{Fe}/\text{H}]$ scale (Carretta & Gratton 1997 in this case) and $[\alpha/\text{Fe}]$ values (the same as in Fig. 13) are not critical, due to the small variation of the predicted R_{bump} in the relevant metallicity range. Observational data are well reproduced by theory, with the few discrepant points being representative of clusters with small RGB star samples and/or affected by differential reddening (see the discussion by Bono et al. 2001). Apart from these, 47Tuc (marked as an open circle in Fig. 14) is the only cluster in clear disagreement with theory, in spite of the large sample of RGB stars observed, and deserves further detailed investigations.

8.3. The RGB Bump as a diagnostic of partial mixing processes.

Cassisi, Salaris & Bono (2002) have recently shown that the RGB bump can be used to test not only the predicted size of the H-jump left over by the convective boundary at its maximum extension, but also the sharpness of this discontinuity. Canonical models and even models with overshooting – as long as the mixing in the overshooting region is assumed to be instantaneous – predict a sharp discontinuity of the H-profile. Conversely, any kind of non-instantaneous transport mechanism acting between the base of the convective envelope and a deeper region (where the local H abundance is no longer equal to the envelope value) which is able to build up abundance gradients, will smooth this sharp discontinuity, and affect the shape of the bump region in the LF (see also Bono & Castellani 1992).

Cassisi et al. (2002) have computed models that simulate the occurrence of partial mixing processes at the bottom of the convective envelope of RGB stars. In particular, they have artificially modified the chemical element profiles of a model at the first dredge-up

stage, smoothing out the sharp H-jump by means of a linear interpolation between the chemically homogeneous envelope and a region below the H-discontinuity. Different smoothing lengths – parametrized as a function of the local pressure scale height – have been considered, and some representative results are shown in Fig. 15. The bump shape produced by canonical models appears asymmetric when the bin size is kept sufficiently small and photometric errors are neglected, with its characteristic peak located in the brightest bump region. By applying some smoothing of the chemical discontinuity, the variations in the shapes of the LF bump are quite evident: when the smoothing length increases the bump becomes more centrally peaked and more symmetric. This occurrence is a consequence of the changes in the evolutionary rate of the H-burning shell when it encounters the H-discontinuity (see Cassisi et al. 2002 for more details). Larger smoothing regions imply a smoother discontinuity in the H-profile (and in the molecular weight profile), and a smaller change in the efficiency of the H-burning shell. In particular, the narrowing of the bump width is related to the decrease of the luminosity drop occurring on the corresponding evolutionary track.

The agreement between predicted and observed R_{bump} values also puts constraints to the maximum possible extension of the partial mixing region, which increases the He abundance in the envelope, thus reducing the overall jump in the H abundance and modifying the value of R_{bump} . Smoothing lengths much larger than $1H_p$ can be ruled out by the R_{bump} test. Also the brightness level of the bump is modified by this process, becoming dimmer by ≈ 0.025 mag for a variation by $0.1H_p$ of the smoothing length.

Data plotted in Fig. 15 show that smoothing lengths equal to or larger than $0.5H_p$ affect significantly the shape of the LF bump. To check if this effect is detectable with real GC data, Cassisi et al. (2002) have performed extensive Monte-Carlo simulations showing that in metal-rich GCs ($[M/H] \approx -1.0$) not affected by differential reddening, the effect of

smoothing lengths equal or larger than $0.5H_P$ can be detected with stellar samples larger than ≈ 120 objects within ± 0.20 mag of the bump peak, a bin size of at most 0.06 mag and 1σ photometric errors not larger than 0.03 mag (see Fig. 15). These requirements can be met, at least for the more massive, metal-rich GCs, by using the new Advanced Camera for Surveys (Clampin et al. 2000) on board the HST.

8.4. The RGB luminosity function heap

Ground based and HST observations of a large sample of RGB stars in NGC 2808 reported by Bedin et al. (2000), have led to the discovery of an additional bump in the LF of the GC NGC 2808 (see Fig. 16). This bump, termed ‘heap’, appears at visual magnitudes ≈ 1.4 mag brighter than the expected bump, and it is present both in the HST data – containing the central regions of the cluster – and in the ground-based data. From a preliminary analysis, this feature appears real and, apparently, lends support to the evidence that a similar heap is also present in the HST data for the cluster 47 Tuc (Bedin et al. 2000).

Canonical RGB stellar models do not predict any decrease of the evolutionary rate able to produce an increase in the star counts in the relevant region of the RGB. If the heap is assumed to be due to a change in the efficiency of H-burning, it could be interpreted as the byproduct of a deep-mixing episode, which somehow causes a temporary delay in the advancement of the H-shell. If this is the case, the LF heap could be adopted to constrain the extension of this deep-mixing in the stellar envelope. At the moment, one can conclude that if the heap is produced by deep-mixing processes, canonical stellar models underestimate the evolutionary lifetime during this phase by about 25%.

However, Bedin et al. (2000) have noticed that, in the case of 47 Tuc, the position of

the heap in the LF is similar to the location of the K Giant Variables (KGVs) discovered in this cluster by Edmonds & Gilliland (1996). If the connection between the LF heap and the presence of the KGVs were to be confirmed by further observations, the heap could be simply related to the position along the RGB of the KGV instability strip and to their properties during the pulsational cycle.

9. The TRGB as standard candle

As discussed in §3, the I -band magnitude of the TRGB appears to be a very good standard candle. Its predicted value depends on the TRGB bolometric magnitude derived from the models which, in turn, depends on the size of the He-core at the He-flash, and it is influenced by any uncertainty affecting the equation of state of partially electron degenerate matter, neutrino energy losses, electron conduction opacity, and the nuclear cross section for the 3α -reaction.

In Fig. 17 we show a comparison of the most recent results concerning the TRGB bolometric magnitude and M_{core}^{He} at the He-flash; the displayed quantities refer to a $0.8M_{\odot}$ model and various initial metallicities (scaled solar metal distribution). M_{bol}^{TRGB} values have all been computed from $\log(L/L_{\odot})$ transformed into M_{bol} , assuming in each case $M_{bol,\odot}=4.75$. This is equivalent of having a BC_V scale in which $BC_{V,\odot} = -0.07$.

There exists fair agreement among the various predictions of the M_{bol}^{TRGB} metallicity dependence, and all the M_{bol}^{TRGB} values at a given metallicity are in agreement within ~ 0.10 mag, with the exception of the P00 and YY01 models, which appear to be underluminous with respect to the others. As for the P00 models this difference follows from their smaller M_{core}^{He} values; it is worth noticing that the recent models by Salasnich et al. (2000), which are an update of the P00 ones, provide brighter M_{bol}^{TRGB} , similar to the V00 results. In case

of the YY01 results the fainter TRGB luminosity cannot be explained by much smaller M_{core}^{He} values, since this quantity is very similar to V00 results.

If one neglects for a moment the P00 and YY01 models, the reason for the 0.1 mag spread among the rest of the authors is mainly due to the electron conduction opacities. The V00 (and Salasnich et al. 2000) models employ the HL69 data, while the other models use the I83 result. Taking into account the effect of different choices for the opacities, the corresponding M_{core}^{He} values would agree within $0.01M_{\odot}$ and the difference in M_{bol}^{TRGB} would further reduce .

As a reference, we show here the relationship from the SC98 models (using $M_{bol,\odot}=4.75$):

$$M_{bol}^{TRGB} = -3.949 - 0.178[M/H] + 0.008[M/H]^2 \quad (4)$$

This relationship covers the metallicity range $-2.35 \leq [M/H] \leq -0.28$, which encompasses the whole metallicity range spanned by galactic GCs.

9.1. Observational tests

Salaris & Cassisi (1997) and Caloi et al. (1997) have discussed an important test for the consistency of theoretical TRGB brightness and He-core masses with observations. They have used the FPC83 estimates of the apparent bolometric TRGB magnitude of various GCs, obtained by directly integrating the flux received from their program stars via the observed UBVIJK photometry. After correcting these magnitudes for the GC distance moduli obtained using the distance scale provided by their ZAHB models, these authors have compared the theoretical M_{bol}^{TRGB} values with the observed ones. This is essentially a comparison of the consistency between the theoretical TRGB and ZAHB distance scales; the importance of this test is due to the fact that the ZAHB and TRGB brightnesses

depend in a different way on the value of M_{core}^{He} and stellar metallicity. Consistency among them provides a strong indication of the reliability of the models.

Figure 18 shows a comparison between the FPC83, together with the more recent Ferraro et al. (2000) data, and the theoretical relationship given above (which is on the same scale as the bolometric magnitude provided by the quoted papers), using the ZAHB distance scale given by the same SC98 models. The solid line represents the theoretical M_{bol}^{TRGB} value, while the dashed lines mark M_{bol}^{TRGB} values increased at steps of 0.1 mag, to show how the observational data are distributed in the various magnitude intervals.

All observational points lie below the theoretical value, being on average about 0.10-0.20 mag underluminous. This is exactly what is expected in case of consistency between the ZAHB and TRGB distance scale, since, given the size of the RGB star samples observed by FPC83 and the evolutionary timescales close to the TRGB, it is statistically unlikely to have detected a star exactly at the TRGB (see, e.g., the discussions in Raffelt 1990, Castellani, Degl’Innocenti & Luridiana 1993, Salaris & Cassisi 1997). Caloi, D’Antona & Mazzitelli (1997) obtained the same results with their RGB and ZAHB models.

This comparison enables us to perform another independent test for the efficiency of deep mixing in RGB stars (see §7). Sweigart (1997a) has computed some evolutionary models for low-mass RGB stars considering mixing of some helium from the H-burning shell into the envelope. A consequence of this mixing is to increase both the TRGB and the ZAHB luminosity level. By parametrizing the efficiency of the deep mixing in term of the amount of hydrogen ΔX_{mix} carried into the H-shell, Sweigart found that $\log L_{TRGB} \approx 0.8\Delta X_{mix}$ and $\log L_{HB} \approx 1.5\Delta X_{mix}$. Since the HB is twice as sensitive as the the TRGB to the efficiency of this extra mixing process, one should expect that the comparison between ZAHB and TRGB distances discussed before could constrain the efficiency of this mechanism, if to occur at all. Assuming all stars in a given cluster

experience this mixing process, for a given value of ΔX_{mix} the ZAHB brightness increases more than the TRGB one, thus moving upwards the TRGB absolute brightness with respect to the theoretical prediction. In the bottom panel of Fig. 18, we show this comparison in the case of $\Delta X_{mix} = 0.10$. On average the observed TRGB magnitude is now equal to the theoretical one, showing that, on the basis of this test alone, $\Delta X_{mix} = 0.10$ is a firm upper limit to the deep mixing efficiency (see also §7.3) ⁸.

9.2. The TRGB absolute brightness calibration

I-band TRGB distance estimates are routinely obtained for Local Group galaxies, and the use of the HST capabilities has allowed the Leo I group and Virgo to be reached (e.g., Sakai et al. 1997, Harris et al. 1998). Madore & Freedman (1995) have discussed the observational requirements for obtaining reliable and unbiased TRGB detections.

The absolute value of the TRGB distances depends, of course, on the absolute calibration of M_{bol}^{TRGB} and the value of the bolometric correction to the *I* band (BC_I). As previously discussed, the large majority of current RGB models predict M_{bol}^{TRGB} values showing a total dispersion of only ~ 0.10 mag, and a dependence on the metallicity which is in fair agreement among various authors. To compare various theoretical determinations of the TRGB distance scale at a fixed metallicity, e.g., the average metallicity of the RGB stellar population in the GC ω Cen ($[Fe/H] \approx -1.7$, see Bellazzini, Ferraro & Pancino 2001

⁸It is worth recalling that the same kind of test has been performed in other investigations, in order to put firm constraints on additional physical effects affecting the size of the He-core at the He-flash, such as the neutrino electromagnetic properties (Raffelt 1990, Raffelt & Weiss 1992, Castellani & Degl’Innocenti 1993), and extra spatial dimensions (Cassisi et al. 2000).

– the reason for this choice will be clear in the following), we will adopt the empirical $BC_I - (V - I)$ relationship by Da Costa & Armandroff (1990 – which is on a scale where $BC_{V,\odot} = -0.07$), and the relationship between $(V - I)_0^{TRGB}$ and $[\text{Fe}/\text{H}]$ from Bellazzini et al. (2001). By assuming $[\alpha/\text{Fe}] = 0.3$ and using Eq. 2, the various theoretical calibrations in fig. 17, with the exception of the YY01 and P00 models, provide M_I^{TRGB} values ranging from -4.22 (Cassisi et al. 1998) to -4.10 (V00). The models of YY01 and P00 provide, respectively, $M_I^{\text{TRGB}} = -4.00$ and -3.95 . As a reference, the M_{bol}^{TRGB} relationship by SC98 given before provides $M_I^{\text{TRGB}} = -4.18$, while the widely used semiempirical calibration by LFM93 gives $M_I^{\text{TRGB}} = -4.00$. This difference is easy to explain. The LFM93 relationship is based on a sample of clusters for which FPC83 m_{bol}^{TRGB} data are available; the metallicity dependence is taken from theoretical models, while the zero point is based on the FPC83 m_{bol}^{TRGB} values corrected for distance moduli provided by a HB brightness scale which is ~ 0.1 mag fainter than the SC98 one. It is evident, on the basis of the previous discussion, that on average the FPC83 empirical data underestimate the true apparent TRGB brightness, and this occurrence accounts for another ~ 0.1 mag of difference between the SC98 and LFM93 calibrations. It is also worth mentioning that the use of theoretical bolometric corrections instead of the empirical Da Costa & Armandroff (1990) ones, change the theoretical M_I^{TRGB} values by about ± 0.05 mag.

Very recently, Bellazzini et al. (2001) have published an independent empirical recalibration of M_I^{TRGB} , based on the globular cluster ω Cen. They adopted the distance obtained by Thompson et al. (2001) from the analysis of an eclipsing binary system in the cluster, and determined the TRGB apparent I brightness from a well populated CMD. The number of stars in the upper RGB appears to be large enough to provide an unbiased estimate of the TRGB level. From their assumed distance modulus and cluster reddening, $M_I^{\text{TRGB}} = -4.04 \pm 0.12$ is obtained. All of the theoretical results mentioned above (coupled with the empirical bolometric corrections by Da Costa & Armandroff 1990) are within 1.5σ

of this calibration.

10. Conclusions

RGB theoretical models play a key role in the interpretation of various astrophysical observations. We have discussed in detail the theoretical uncertainties still affecting the models, paying particular attention to the predictions of colors, luminosities, evolutionary timescales and surface chemical abundances. A comparison of various theoretical RGB models with a large body of diverse empirical data has allowed us to discuss not only the accuracy of the adopted input physics, but also the adequacy of the assumptions built into canonical RGB models.

Large uncertainties still exist in the predictions of T_{eff} and colors, due mainly to the treatment of superadiabatic convection, boundary conditions and color transformations employed; they can however be minimized by a suitable calibration of the models on empirical data. The prediction of the absolute value of the He-core mass at the He-flash – which determines the TRGB and HB brightness – suffers from residual uncertainties mainly related to the determination of accurate electron conduction opacities in the relevant physical regime.

Extra mixing processes not included in canonical RGB models seem to be required to help explaining some of the chemical abundance patterns observed at the photosphere of RGB stars; however, independent empirical constraints, and arguments from stellar nucleosynthesis require that these processes should not be able to affect appreciably the evolutionary timescales, He-core masses and CMD location obtained from canonical models.

We wish to warmly thank V. Castellani and D. Vandenberg for very useful comments on an early version of the manuscript, which greatly improved the quality of this review, as

well as for valuable suggestions and discussions on the subject. We also thank G. Bono, L. Girardi, P. James, S. Percival and L. Piersanti for an accurate reading of the manuscript. We are grateful to F. D’Antona, D. Vandenberg and S. Yi for providing us with their results, and to M. Bellazzini, B. Chaboyer, H. Schlattl for useful discussions.

A.W. likes to thank P. Denissenkov for his collaboration, R. Kraft and R. Peterson for many stimulating discussions and advices, and S. Goriely for providing Fig. 9. S.C. acknowledges the financial support by MURST (Cofin2000) under the scientific project: “Stellar observables of cosmological relevance” and by (Cofin2001) under the scientific project: “Origin and evolution of stellar populations in the galactic spheroid”.

REFERENCES

- Achatz, K., 1995, *Dynamik thermonuklearer Verbrennungsvorgänge im “core helium flash”*,
Diplomarbeit, Techn. University Munich
- Aikawa, M., Fujimoto, M. Y., & Kato, K., 2001, *ApJ*, 560, 937
- Alexander, D.R., & Ferguson, J.W., 1994, *ApJ*, 437, 879
- Alongi, M., Bertelli, G., Bressan, A., & Chiosi, C., 1991, *A&A*, 244, 95
- Alonso, A., Arribas, & Martinez-Roger, C., 1996, *A&A*, 313, 873
- Alonso, A., Arribas, & Martinez-Roger, C., 1999, *A&AS*, 140, 261
- Alonso, A., Salaris, M., Arribas, S., Martinez-Roger, C., & Asensio Ramos, A., 2000, *A&A*,
355, 1060
- Alves, D. R., & Sarajedini, A., 1999, *ApJ*, 511, 225
- Arnould, M., Goriely, S., & Jorissen, A., 1999, *A&A*, 347, 572
- Bedin, L. R., Piotto, G., Zoccali, M., Stetson, P. B., Saviane, I., Cassisi, S., & Bono, G.,
2000, *A&A*, 363, 159
- Bell, R.A., Dickens, R.J., & Gustafsson, B., 1979, *ApJ*, 229, 604
- Bellazzini, M., Ferraro, F. R., & Pancino, E., 2001, *ApJ*, 556, 635
- Bellman, S., Briley, M.M., Smith, G.H., & Claver, C.F., 2001, *PASP*, 113, 326
- Bergbusch, P.A., & Vandenberg, D.A., 2001, *ApJ*, 556, 322
- Böhm-Vitense, E., 1958, *ZAp*, 46, 108
- Bono, G., Cassisi, S., Zoccali, M., & Piotto, G., 2001, *ApJ*, 546, L109

- Bono, G., & Castellani, V., 1992, A&A, 258, 385
- Briley, M.M., Bell, R.A., Hoban, S., & Dickens, R.J., 1990, ApJ, 359, 307
- Briley, M.M. & Cohen, J.G., 2001, AJ, 122, 242
- Briley, M.M., Smith, G.H., & Claver, C.F., 2001, AJ, 122, 2561
- Buser, R., & Kurucz, R.L., 1992, A&A, 264, 557
- Caloi, V., D'Antona, F., & Mazzitelli, I., 1997, A&A, 320, 823
- Cannon, R.D., Croke, B. F.W., Bell, R.A., Hesser, J.E., & Stathakis, R.A., 1998, MNRAS, 298, 601
- Canuto, V.M., & Mazzitelli, I., 1991, ApJ, 370, 295
- Canuto, V.M., Goldman, I., & Mazzitelli, I., 1996, ApJ, 473, 550
- Carbon, D.F., et al., 1982, ApJS, 49, 207
- Carney, B. W., 1996, PASP, 108, 900
- Carretta, E., & Gratton, R. G., 1997, A&AS, 121, 95
- Cassisi, S., & Salaris, M., 1997, MNRAS, 285, 593
- Cassisi, S., Salaris, M., & Bono, G., 2002, ApJ, *in press*, (astro-ph/0110247)
- Cassisi, S., Castellani, V., Degl'Innocenti, S., & Weiss, A., 1998, A&AS, 129, 267
- Cassisi, S., Castellani, V., Degl'Innocenti, S., Fiorentini, G., & Ricci, B., 2000, Phys. Lett. B, 481, 323
- Castellani, M., & Castellani, V., 1993, ApJ, 407, 649

- Castellani, V., Chieffi, A., & Norci, L., 1989, *A&A*, 216, 62
- Castellani, V., & Degl’Innocenti, S., 1993, *ApJ*, 402, 574
- Castellani, V., & Degl’Innocenti, S., 1999, *A&A*, 344, 97
- Castellani, V., Degl’Innocenti, S., & Luridiana, V., 1993, *A&A*, 272, 442
- Castellani, V., Ciaccio, F., Degl’Innocenti, S., & Fiorentini, S., 1997, *A&A*, 322, 801
- Castellani, V., Degl’Innocenti, S., Girardi, L., Marconi, M., Prada Moroni, P. G., & Weiss, A., 2000, *A&A*, 354, 150
- Castelli, F., 1999, *ApJ*, 346, 564
- Castelli, F., Gratton, R.G., & Kurucz, R.L., 1997, *A&A*, 318, 841
- Castilho, B.V., Pasquini, L., Allen, D.M., Barbuy, B., & Molaro, P., 2000, *A&A*, 361, 92
- Catelan, M., 2000, *ApJ*, 521, 826
- Catelan, M., de Freitas Pacheco, J.A., & Horvath, J.E., 1996, *ApJ*, 461, 231
- Caughlan, G.R., & Fowler, W.A., 1988, *Atom. Data Nucl. Data Tables*, 40, 283
- Cavallo, R.M., Sweigart, A.V., & Bell, R.A., 1998, *ApJ*, 492, 575
- Chaboyer, B., & Kim, Y.-C., 1995, *ApJ*, 454, 767
- Charbonnel, C., 1995, *ApJ*, 453, L41
- Charbonnel, C., Brown, J.A., & Wallerstein, G., 1998, *A&A*, 332, 204
- Charbonnel, C. & do Nascimento, J.D., 1998, *A&A*, 336, 915
- Clampin, M., & ACS Science Team, 2000, *BAAS*, 197, 1218

- Da Costa, G.S., 1998, in ‘Fundamental Stellar Properties: the interaction between observation and theory’, T.R. Bedding, A.J. Booth, & J. Bavis eds., IAU Symp. No. 189 (Dordrecht: Kluwer), 193
- Cox, J.P., & Giuli, R.T., 1968, ‘Principles of Stellar Structure’, (New York: Gordon and Breech)
- Da Costa, G.S., & Armandroff, T.E., 1990, AJ, 100, 162
- Däppen, W., Mihalas, D., Hummer, & D. G., Mihalas, B.W., 1988, ApJ, 332, 261
- D’Cruz, N.L., Dorman, B., Rood, R.T., & O’Connell, R.W., 1996, ApJ, 466, 359
- Degl’Innocenti, S., Dziembowski, W.A., Fiorentini, G., & Ricci, B., 1997, A Ph, 7, 77
- Demarque, P., & Mengel, J. G., 1972, ApJ, 171, 583
- Denissenkov, P.A., Da Costa, G.S., Norris, J.E., & Weiss, A., 1998, A&A, 333, 926
- Denissenkov, P.A., & Denissenkova, S.N., 1990, SvA Lett., 16, 275
- Denissenkov, P.A. & Tout, C.A., 2001, MNRAS, 316, 395
- Denissenkov, P.A. & Weiss, A., 1996, A&A, 308, 773
- Denissenkov, P.A. & Weiss, A., 2001, ApJ, 559, L115
- Denissenkov, P.A., Weiss, A., & Wagenhuber, J., 1997, A&A, 320, 115
- Deupree, R.G., 1996, ApJ, 471, 377
- De Witt, H.E., Graboske, H.C., & Cooper, M.S., 1973, ApJ, 181, 439
- Edmonds, P. D., & Gilliland, R. L., 1996, ApJ, 464, L157
- Eggleton, P., 1968, MNRAS, 140, 387

- Fernie, J.D., 1983, *PASP*, 95, 782
- Ferraro, F. R., Messineo, M., Fusi Pecci, F., de Palo, M. A., Straniero, O., Chieffi, A., & Limongi, M., 1999, *AJ*, 118, 1738
- Ferraro, F. R., Montegriffo, P., Origlia, L., & Fusi Pecci, F., 2000, *AJ*, 119, 1282
- Fowler, W.A., Caughlan, G.R., & Zimmermann, B.A., 1975, *ARA&A*, 13, 69
- Freytag, B., & Salaris, M., 1999, *ApJ*, 513, L49
- Frogel, J.A., Persson, S.E. & Cohen, J.G., 1983, *ApJS*, 53, 713
- Fusi Pecci, F., Ferraro, F. R., Crocker, D. A., Rood, R. T., & Buonanno, R., 1990, *A&A*, 238, 95
- Fujimoto, M.Y., Aikawa, M., & Kato, K., 1999, *ApJ*, 519, 733
- Fujimoto, M.Y., Iben, I. Jr., & Hollowell, D., 1990, *ApJ*, 349, 580
- Fujimoto, M.Y., Ikeda, Y., & Iben, I., Jr., 2000, *ApJ*, 529, L25
- Girardi, L., Bressan, A., Chiosi, C., Bertelli, G., & Nasi, E., 1996, *A&AS*, 117, 113
- Girardi, L., Bressan, A., Bertelli, G., & Chiosi, C., 2000, *A&AS*, 141, 371
- Gilroy, K.K., 1989, *ApJ*, 347, 835
- Gonzalez, G. & Wallerstein, G., 1998, *AJ*, 116, 765
- Gratton, R.G., Sneden, C., Carretta, E., & Bragaglia, A., 2000, *A&A*, 354, 169
- Gratton, R. G., et al. 2001, *A&A*, 369, 87
- Graboske, H.C., De Witt, H.E., Grossman, A.S., & Cooper, M.S., 1973, *ApJ*, 181, 457

- Green, E.M., 1988, in ‘Calibration of stellar ages’, A.G. Davis Philip ed. (L. Davis Press), p. 81
- Grevesse, N., & Noels, A., 1993, in ‘Origin and Evolution of the Elements’, N. Prantzos, E. Vangioni-Flam, M Casse eds. (Cambridge: Cambridge University Press)
- Groenewegen, M.A.T, & Salaris, M., 1999, A&A, 348, L33
- Haft, M., Raffelt, G., & Weiss, A., 1994, ApJ, 425, 22
- Harpaz, A., & Kovetz, A., 1988, ApJ, 331, 898
- Harris, W., Durrell, P. R., Pierce, M. J., & Secker, J., Nature, 395, 48
- Hayes, D.S., 1985, in IAU Symp. 111, ‘Calibration of Fundamental Stellar Quantities’, Hayes, D.S., Pasinetti, L.E., Davis Philip, A.G. (eds.), 225
- Hollowell, D., Iben, I. Jr., & Fujimoto, M. Y., 1990, ApJ, 351, 245
- Houdashelt, M.L, Bell, R.A., & Sweigart, A.V., 2000, AJ, 119, 1448
- Hubbard, W.B., & Lampe, M., 1969, ApJS, 163, 297
- Iben, I. Jr., 1968a, ApJ, 154, 581
- Iben, I. Jr., 1968b, Nature, 220, 143
- Iben, I., Jr., 1993, ApJ, 415, 767
- Iben, I, Jr., & Renzini, A., 1984, Phys. Rep., 105, 329
- Iglesias, C.A., & Rogers, F.J., 1996, ApJ, 464, 943
- Itoh, N., Mitake, S., Iyetomi, H., & Ichimaru, S., 1983, ApJ, 273, 774
- Itoh, N., Hayashi, H., Nishikawa, A., Kohyama, Y., 1996, ApJS, 102, 411

- Ivans, I.I., Kraft, R.P., Sneden, C., Smith, G.H., Rich, R.M., & Shetrone, M., 2001, *AJ*, 122, 1438
- Ivans, I.I., Sneden, C., Kraft, R.P., Suntzeff, N.B., Smith, V.V., Langer, G.E., & Fulbright, J.P., 1999, *AJ*, 118, 1273
- Keller, L.D., Pilachowski, C.A., & Sneden, C., 2001, *AJ*, 122, 2554
- King, C. R., Da Costa, G. S., & Demarque, P., 1985, *ApJ*, 299, 674
- King, J.R., Stephens, A., Boesgaard, A.M., & Deliyannis, C.P., 1998, *AJ*, 115, 666
- Kippenhahn, R., & Weigert, A., 1991, in ‘Stellar structure and evolution’, (Berlin: Springer-Verlag)
- Kraft, R.P., 1994, *PASP*, 106, 553
- Krishna-Swamy, K.S., 1966, *ApJ*, 145, 174
- Kurucz, R.L., 1992, in IAU Colloquium 138, ‘Peculiar versus Normal Phenomena in A-Type and related Stars’, ASP Conference Series, vol.44
- Langer, G.E. & Hoffman, R.D., 1995, *PASP*, 107, 1177
- Langer, G.E., Hoffman, R.D., & Sneden, C., 1993, *PASP*, 105, 301
- Langer, G.E., Hoffman, R.D., & Zaidins, C.S., 1997, *PASP*, 109, 244
- Langer, G. E., Bolte, M., & Sandquist, E., 2000, *ApJ*, 529, 936
- Langer, G.E., Kraft, R.P., Carbon, D.F., Friel, E., & Oke, J.B., 1986, *PASP*, 98, 473
- Lee, Y-W, Demarque, P, Zinn, R., 1990, *ApJ*, 350, 155
- Lee, M.G., Freedman, W., & Madore, B.F., 1993, *ApJ*, 417, 553

- Lejeune, T., Cuisinier, V., & Buser, R., 1998, *A&AS*, 130, 65
- Ludwig, H-G, Freytag, B., & Steffen, M., 1999, *A&A*, 346, 111
- Madore, B. F., & Freedman, W. L., 1995, *AJ*, 109, 1645
- Magni, G., & Mazzitelli, I., 1979, *A&A*, 72, 134
- Mazzitelli, I., D’Antona, F., & Caloi, V., 1995, *A&A*, 302, 382
- Mengel, J. G., & Gross, P. G., 1976, *Astrophys. Space Sci.*, 41, 407
- Mihalas, D., 1978, in ‘Stellar atmospheres’, Freeman, San Francisco
- Montegriffo, P., Ferraro, F., Origlia, L., & Fusi Pecci, F., 1998, *MNRAS*, 297, 872
- Montalban, J., Kupka, F., D’Antona, F., & Schmidt, W., 2001, *A&A*, 370, 982
- Munakata, H., Kohyama, Y., & Itoh, N., 1985, *ApJ*, 296, 197
- Neuforge, C., 1993, *A&A*, 274, 818
- Norris, J.E. & Da Costa, G.S., 1995, *ApJ*, 441, L81
- Pedersen, B.B., Vandenberg, D.A., & Irwin A.W., 1990, *ApJ*, 352, 279
- Pilachowski, C. A., Sneden, C., Kraft, R. P., & Langer, G. E., 1996, *AJ*, 112, 545
- Proffitt, C.R., Vandenberg, D.A., 1991, *ApJS*, 77, 473
- Raffelt, G. G., 1990, *ApJ*, 365, 559
- Raffelt, G. G., & Weiss, A., 1992, *A&A*, 264, 536
- Reimers, D., 1975a, in ‘Problems in Stellar Atmospheres and Envelopes’, ed. B. Baschek, W.H. Kegel, & G. Traving (Berlin:Springer-Verlag), 229

- Reimers, D., 1975b, in ‘Problemes D’Hydrodynamique Stellaire’, Memoires de la Societe Royale de Sciences de Liege, 6e serie, tome VIII, 369 p. 149, Geneva: Geneva Obs.
- Renzini, A., & Fusi Pecci, F., 1988, ARA&A, 26, 199
- Renzini, A., & Ritossa, C., 1994, ApJ, 433, 293
- Rogers, F.J., Swenson, F.J., & Iglesias, C.A., 1996, ApJ, 456, 902
- Rood, R. T., Carretta, E., Paltrinieri, B., Ferraro, F. R., & Fusi Pecci, F., 1999, ApJ, 523, 752
- Ross, J.E., & Aller, L.H., 1976, Science, 191, 1223
- Rutledge, G. A., Hesser, J. E., & Stetson, P. B., 1997, PASP, 109, 907
- Sakai, S., Madore, B.F., Freedman, W.L., Lauer, T.R., Ajhar, E.A., & Baum, W.A., 1997, ApJ, 478, 49
- Salaris, M., & Cassisi, S., 1996, A&A, 305, 858
- Salaris, M., & Cassisi, S., 1997, MNRAS, 289, 406
- Salaris, M., & Cassisi, S., 1998, MNRAS, 298, 166
- Salaris, M., & Weiss, A., 1998, A&A, 335, 943
- Salaris, M., Chieffi, A., & Straniero, O., 1993, ApJ, 414, 580
- Salasnich, B., Girardi, L., Weiss, A., & Chiosi, C., 2000, A&A, 361, 1023
- Sandquist, E. L., 2000, MNRAS, 313, 571
- Saviane, I., Rosenberg, A., Piotto, G., & Aparicio, A., 2000, A&A, 355, 966
- Schlattl, H., Cassisi, S., Salaris, M., & Weiss, A., 2001, ApJ, 559, 1082

- Schwarzschild, M., & Härm, R., 1962, ApJ,136, 158
- Schwarzschild, M., & Härm, R., 1964, ApJ,139, 594
- Schwarzschild, M., & Härm, R., 1967, ApJ,150, 961
- Sekiguchi, M., & Fukugita, M., 2000, AJ, 120, 1072
- Shetrone, M.D., 1996a, AJ, 112, 1517
- Shetrone, M.D., 1996b, AJ, 112, 2639
- Silvestri, F, Ventura, P, D’Antona, F, Mazzitelli, I, 1998, ApJ, 509, 192
- Soker, N., Catelan, M., Rood, R.T., & Harpaz, A., 2001, ApJ, 563, L69
- Straniero, O., 1988, A&AS, 76, 157
- Sugimoto, D., 1964, Prog. Theor. Phys., 32, 703
- Sugimoto, D., & Fujimoto, M., 2000, ApJ, 538, 837
- Suntzeff, N.B., 1981, ApJS, 47, 1
- Suntzeff, N.B., & Smith, V.V., 1991, ApJ, 381, 160
- Sweigart, A.V., 1997a, ApJ, 474, L23
- Sweigart, A.V., 1997b, in ‘The Third Conference on Faint Blue Stars’, A. G. D. Philip,
J. Liebert, R. Saffer, & D. S. Hayes eds., IAU Colloq. No. 95 (L. Davis Press)
- Sweigart, A.V., & Gross, P.G., 1978, ApJS, 36, 405
- Sweigart, A.V., & Mengel, J. G., 1979, ApJ, 229, 624
- Sweigart, A.V., Greggio, L., & Renzini, A., 1989, ApJS, 69, 911

- Sweigart, A.V., Greggio, L., & Renzini, A., 1990, *ApJ*, 364, 527
- Thomas, H. C., 1967, *ZAp*, 67, 420
- Thompson, I.B., Kaluzny, J., Pych, W., Burley, G., Krzeminski, W., Paczynski, B., Persson, S.E., & Preston, G.W., 2001, *AJ*, 121, 3089
- Trefzger, D. V., Langer, G. E., Carbon, D. F., Suntzeff, N. B., & Kraft, R. P., 1983, *ApJ*, 266, 144
- Vandenberg, D.A., & Irwin, A.W., 1997, in ‘Advances in Stellar Evolution’, R.T. Rood and A. Renzini eds., Cambridge Univ. Press., p.22
- Vandenberg, D.A., Larson, A.M., & de Propris, R., 1998, *PASP*, 110, 98
- Vandenberg, D.A., Stetson, P.B., Bolte, M., 1996, *ARA&A*, 34, 461
- Vandenberg, D. A., Swenson, F. J., Rogers, F. J., Iglesias, C. A., & Alexander, D. R., 2000, *ApJ*, 532, 430
- Ventura, P., D’Antona, F., Mazzitelli, I., & Gratton, R., 2001, *ApJ*, 550, L65
- von Braun, K., Chiboucas, K., Minske, J.K., Salgado, J.F., & Worthey, G., 1998, *PASP*, 110, 810
- Wasserburg, G. J., Boothroyd, A. I., & Sackmann, I. J., 1995, *ApJ*, 447, L37
- Weiss, A., 1989, *A&A*, 209, 135
- Weiss, A., & Salaris, M., 1999, *A&A*, 346, 897
- Weiss, A., Wagenhuber, J., & Denissenkov, P.A., 1996, *A&A*, 313, 581
- Weiss, A., Cassisi, S., Schlattl, H., & Salaris, M., 2000a, *ApJ*, 533, 413

Weiss, A., Denissenkov, P. A., & Charbonnel, C., 2000b, *A&A*, 356, 181

Worthey, G., 1994, *ApJS*, 95, 107

Yi, S., Demarque, P., Lee, Y-W., Ree, C., Lejeune, T., & Barnes, S., 2001, *ApJS*, 136, 417

Zahn, J-P, 1999, in *ASP Conf. Ser. Vol. 173*, ‘Theory and Tests of Convection in Stellar Structure’, ed. A. Gimenez, E.F. Guinan & B. Montesinos (San Francisco: ASP), 121

Zinn, R., & West, M. J., 1984, *ApJS*, 55, 45

Zoccali, M., & Piotto, G., 2000, *A&A*, 358, 943

Zoccali, M., Cassisi, S., Piotto G., Bono G., & Salaris M., 1999, *ApJ*, 518, L49

Zoccali, M., Cassisi, S., Bono, G., Piotto, G., Rich, R.M., Djorgovski, S. G., 2000, *ApJ*, 538, 289

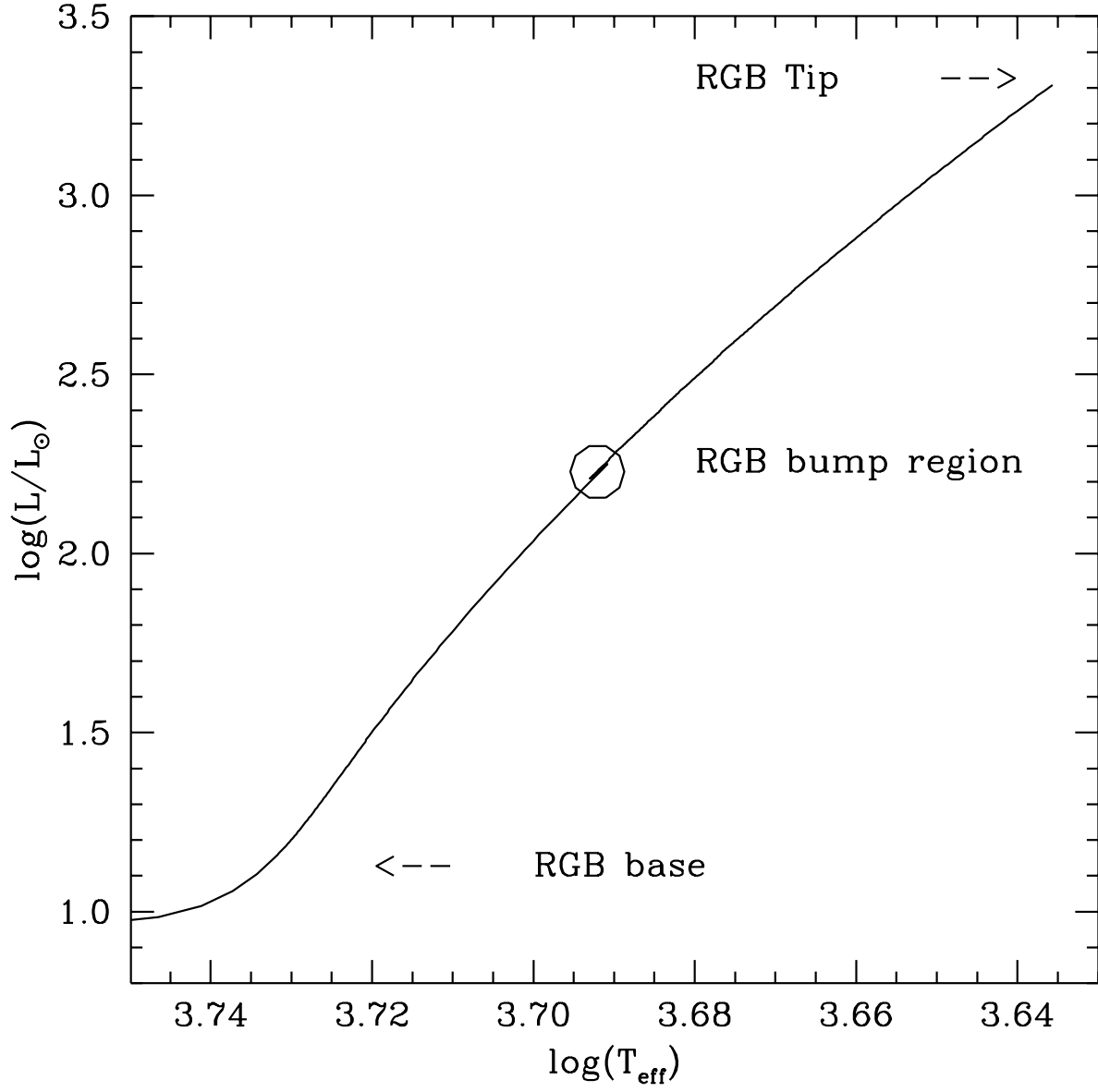


Fig. 1.— RGB evolution in the $\log(L/L_{\odot})/T_{\text{eff}}$ plane of a $1M_{\odot}$ star, $Z=0.0004$ and $Y=0.231$, scaled solar metal distribution.

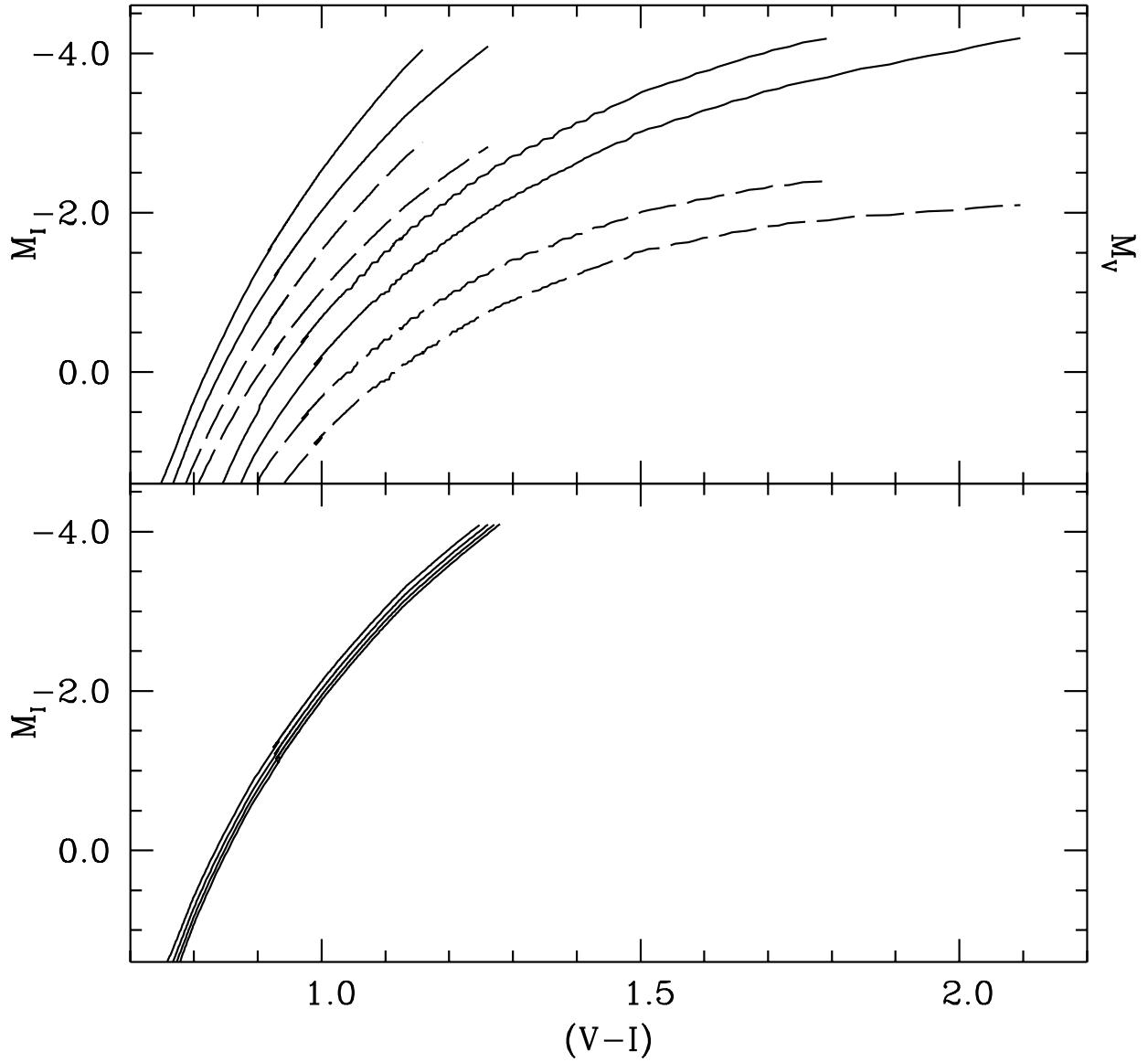


Fig. 2.— RGB isochrones in the $I - (V - I)$ Johnson-Cousins plane (solid lines) and in the $V - (V - I)$ plane (dashed lines). The upper panel shows 10 Gyr isochrones with $Z=0.0002$, 0.0004, 0.004, 0.008 (from left to right). The lower panel displays $Z=0.0004$ isochrones with ages of 8, 10, 12, 14 Gyr.

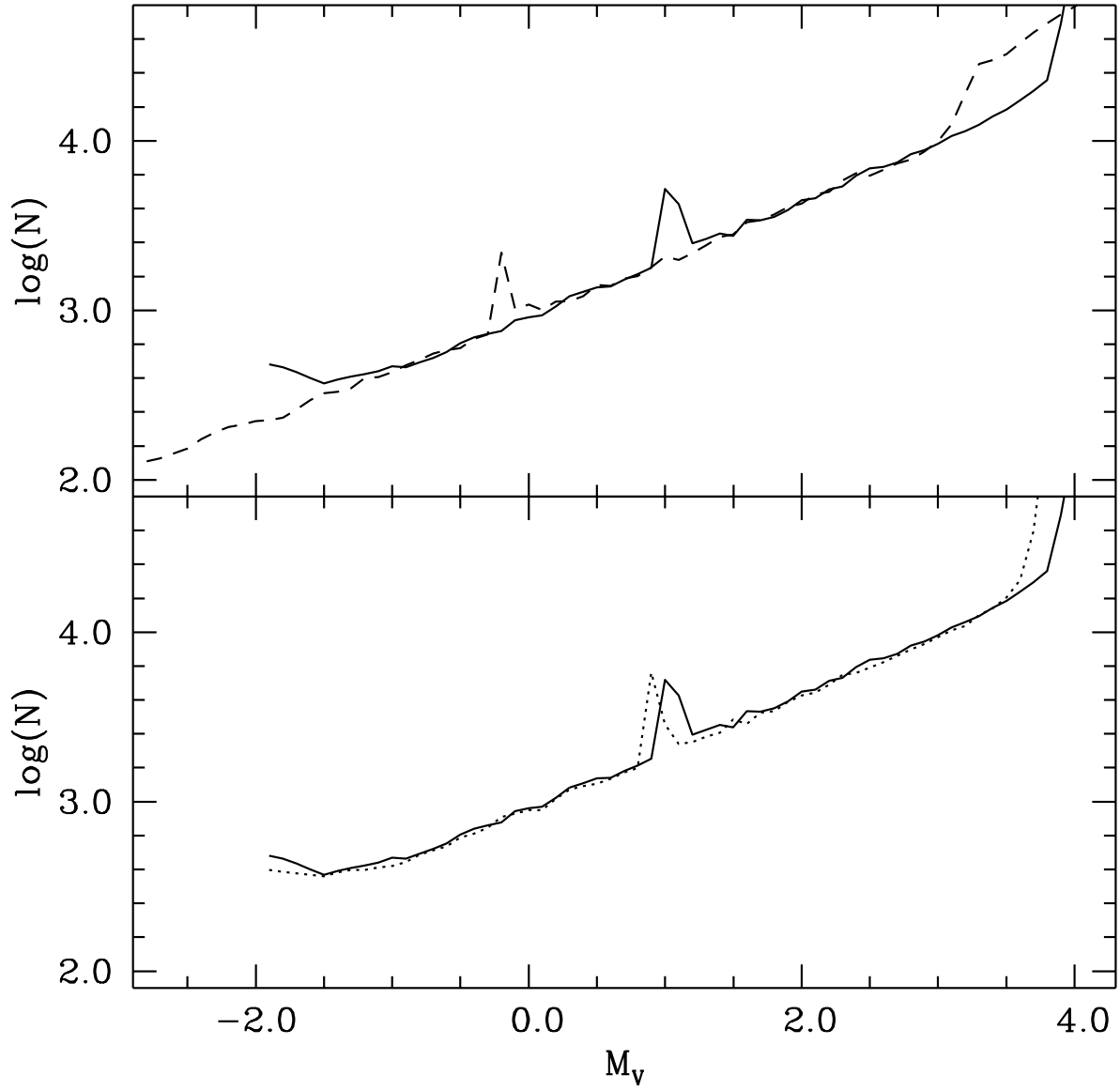


Fig. 3.— The upper panel shows a comparison of 13 Gyr LFs with $Z=0.008$ (solid line) and $Z=0.0004$ (dashed line); the lower panel displays two LFs with $Z=0.008$ and $t=10$ (dotted line) and 13 (solid line) Gyr.

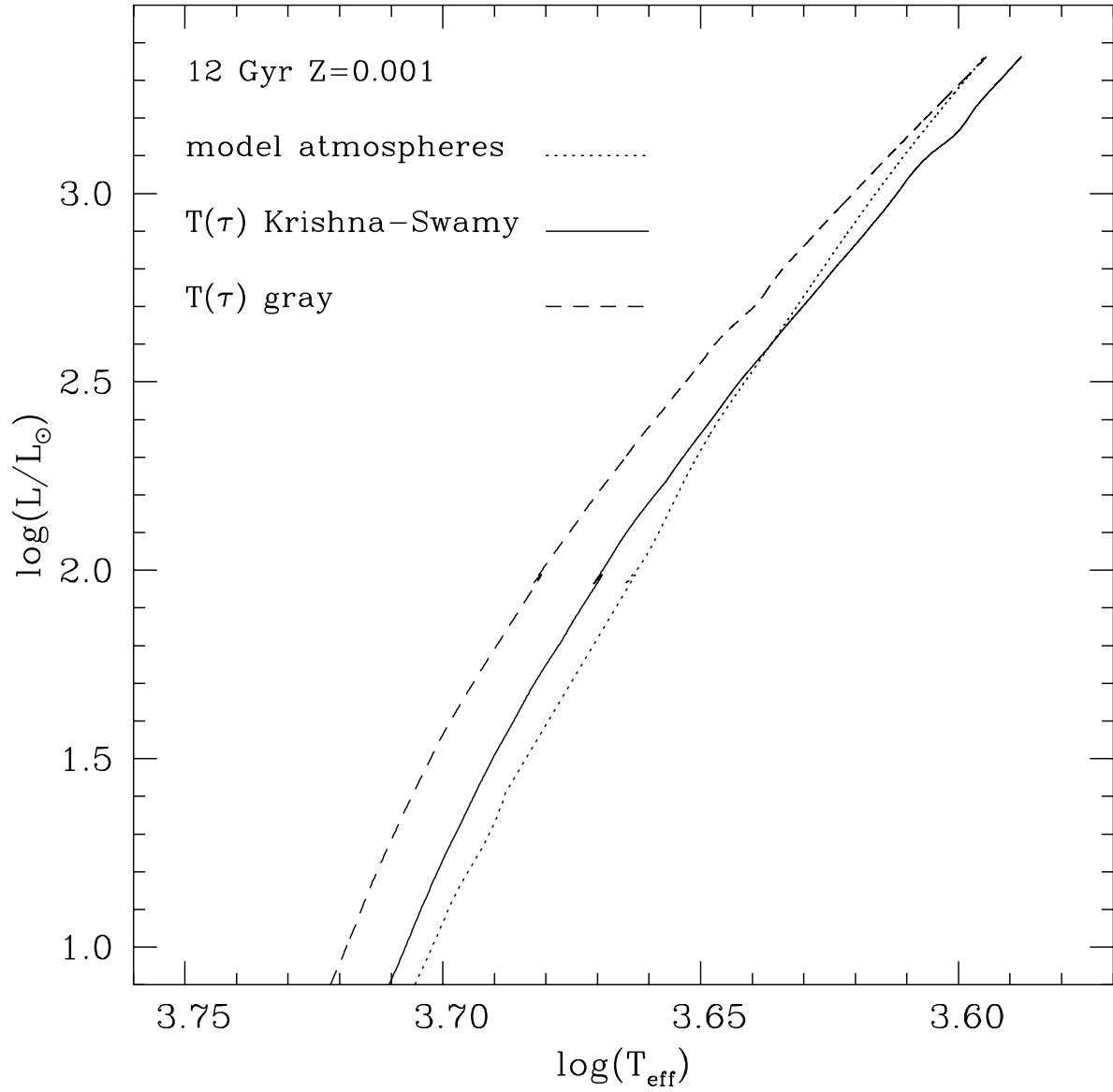


Fig. 4.— Comparison of 12 Gyr RGB models for $Z=0.001$, computed using model atmospheres (dotted line) and, respectively, gray (dashed line) and Krishna-Swamy (1966 – solid line) $T(\tau)$ relationships to obtain the surface boundary conditions. See text for details.

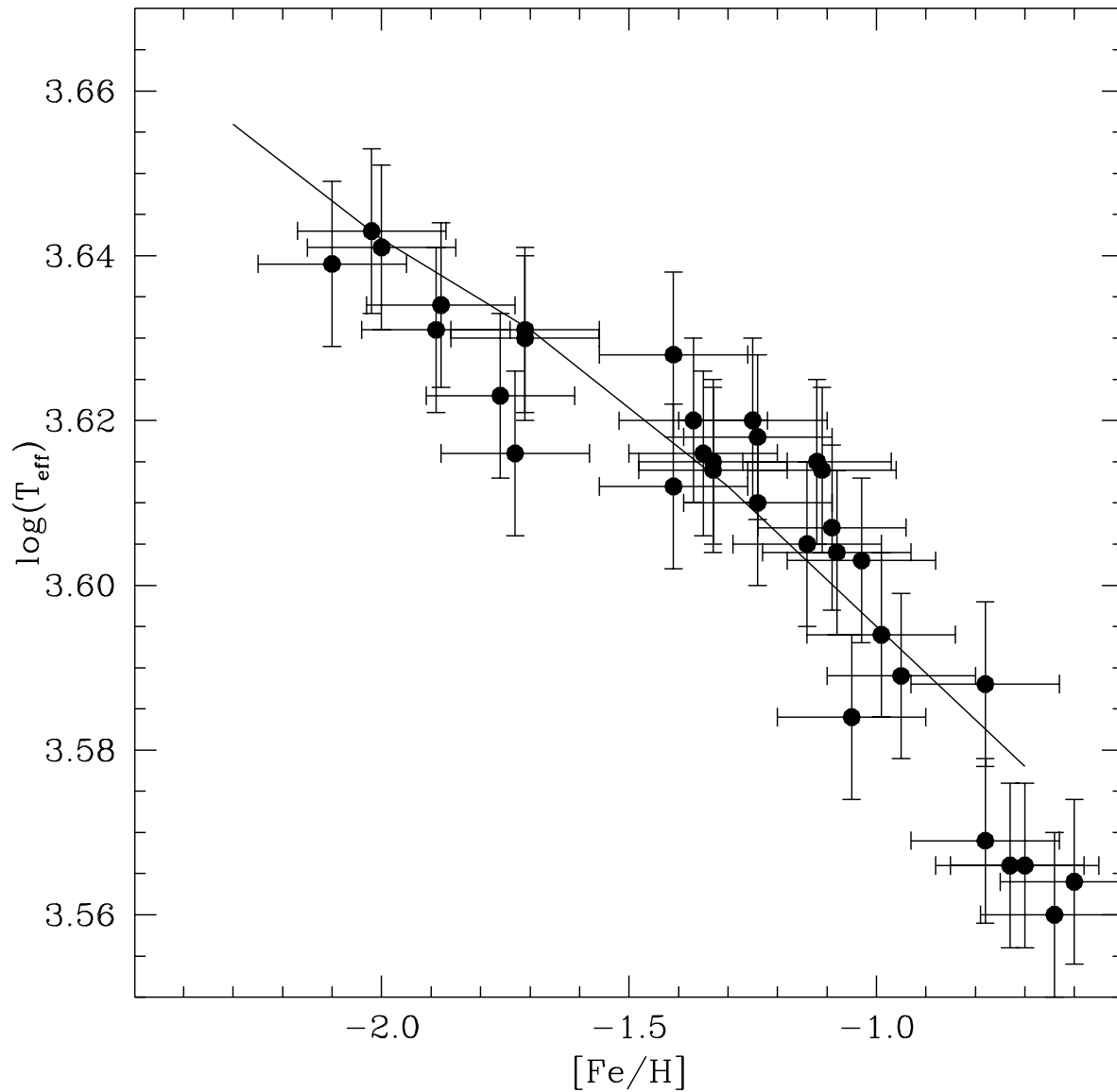


Fig. 5.— RGB T_{eff} (at $M_{\text{bol}} = -3$) as a function of $[\text{Fe}/\text{H}]$ from Salaris & Weiss (1998) 12 Gyr α -enhanced ($[\alpha/\text{Fe}]=0.4$) isochrones (solid line), compared with globular clusters T_{eff} from Frogel, Persson & Cohen (1983), and $[\text{Fe}/\text{H}]$ from Carretta & Gratton (1997). Displayed error bars are of 100 K in T_{eff} and 0.15 dex in $[\text{Fe}/\text{H}]$.

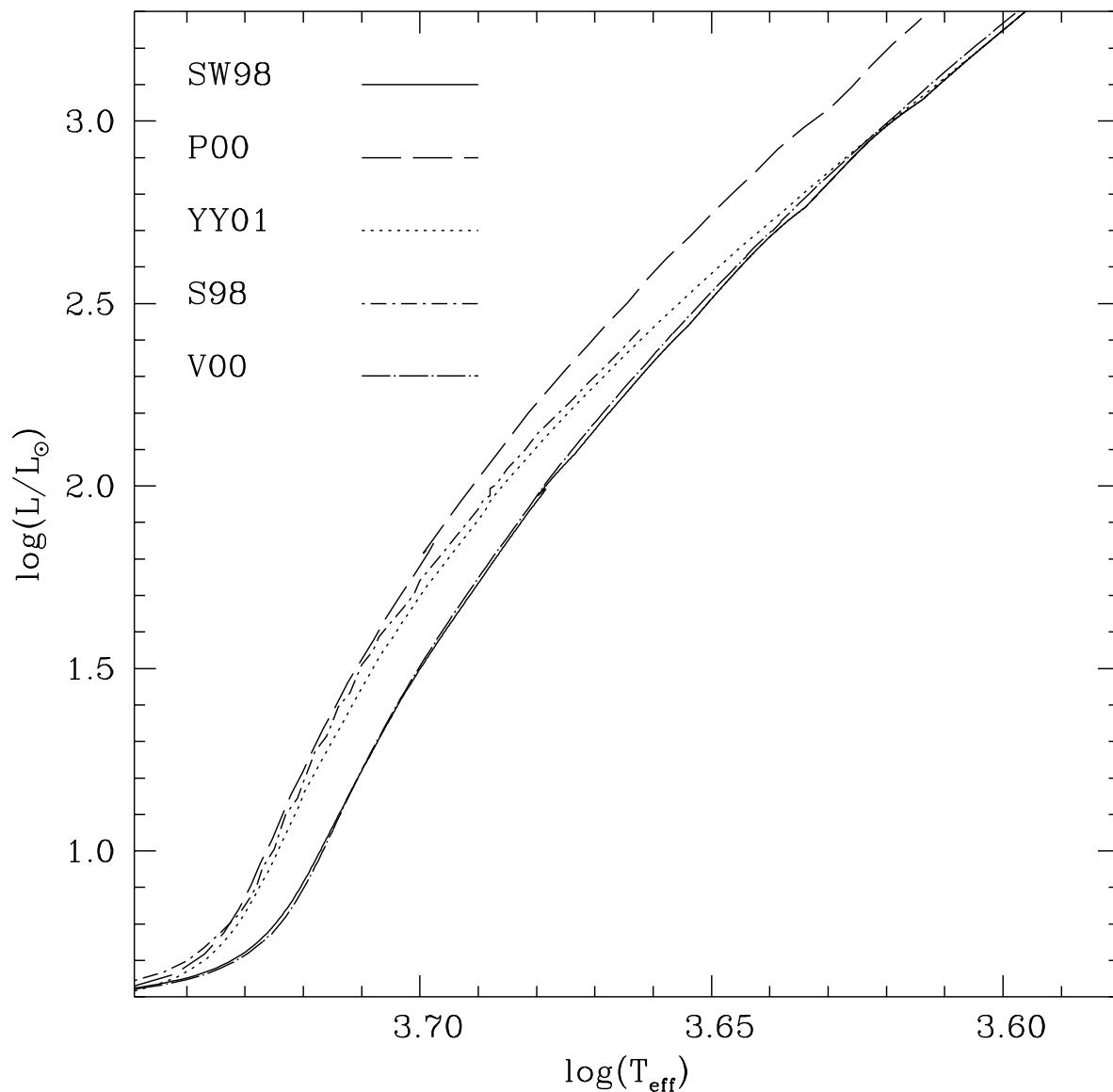


Fig. 6.— RGB isochrones computed with a solar calibrated α_{MLT} for a scaled-solar $Z=0.001$ metal mixture and $t=12$ Gyr, from different sources: Girardi et al. (2000 – P00); Yonsei-Yale models (Yi al. 2001 – YY01); Vandenberg et al. (2000 – V00); scaled solar models computed with the same input physics as in Salaris & Weiss (1998 – SW98); FST models by Silvestri et al. (1998 – S98).

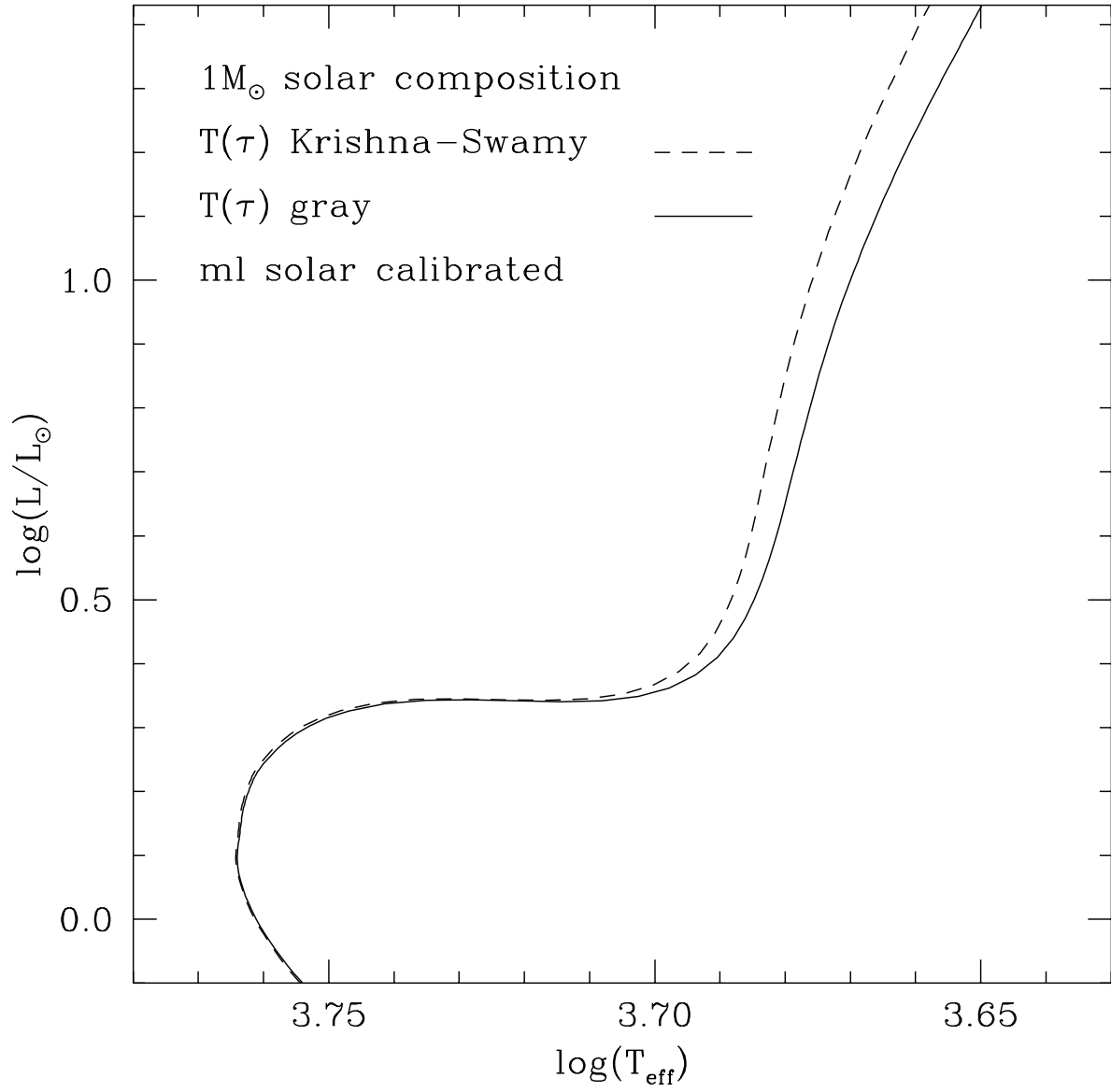


Fig. 7.— Two models for a $1M_{\odot}$ star, solar chemical composition and α_{MLT} , and two different $T(\tau)$ relationships.

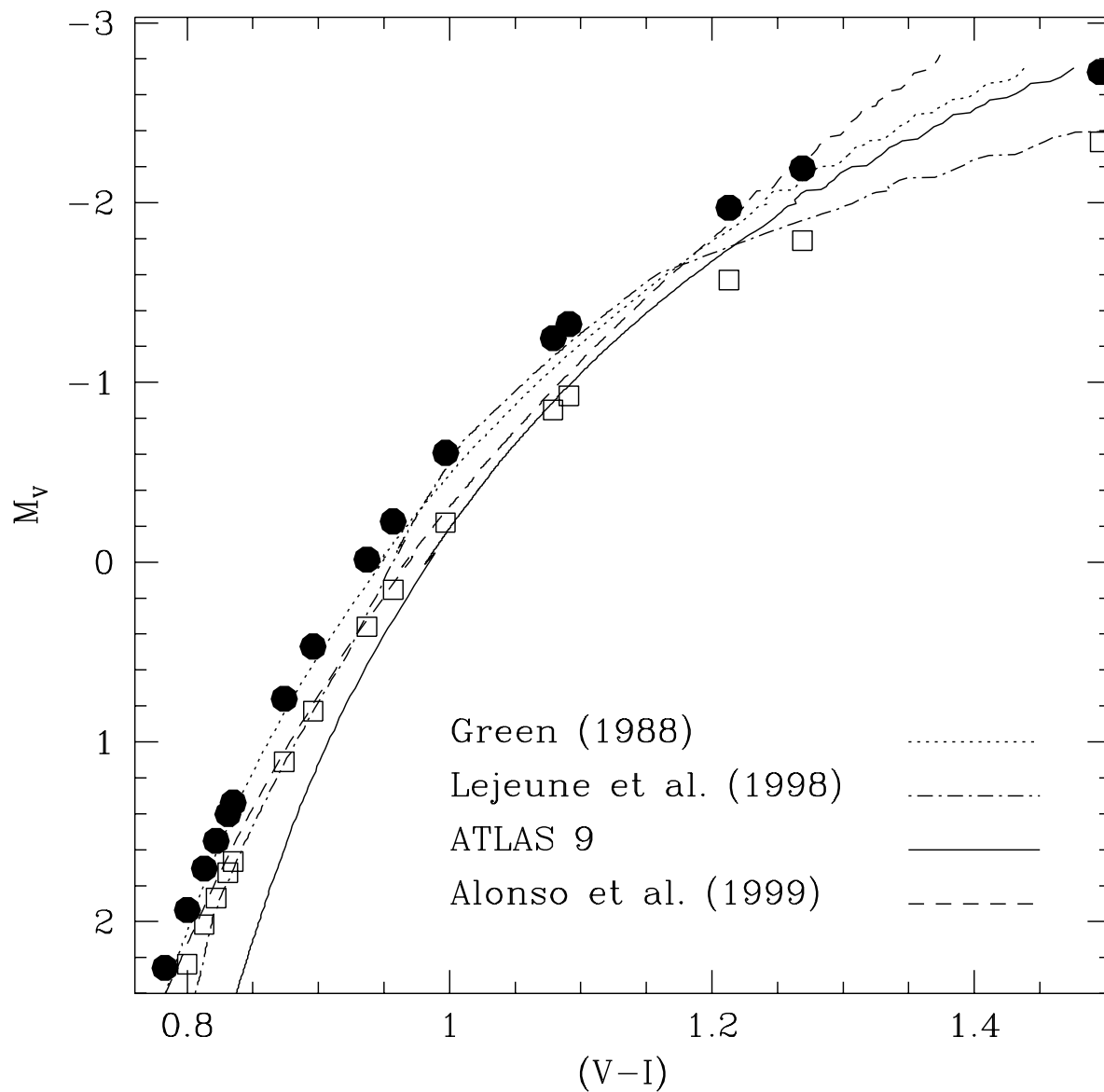


Fig. 8.— An isochrone with $t=10$ Gyr and $Z=0.001$ (from SW98) transformed to the $V - (V - I)$ plane using the 4 sets of transformations discussed in the text. Filled circles and empty squares denote the RGB location (from Saviane et al. 2000) of Galactic GCs with this metallicity (assuming the same $[\alpha/\text{Fe}]$ as in the SW98 models), considering both the Carretta & Gratton (1997 – filled circles) and Zinn & West (1984 – empty squares) $[\text{Fe}/\text{H}]$ scales (see text for more details).

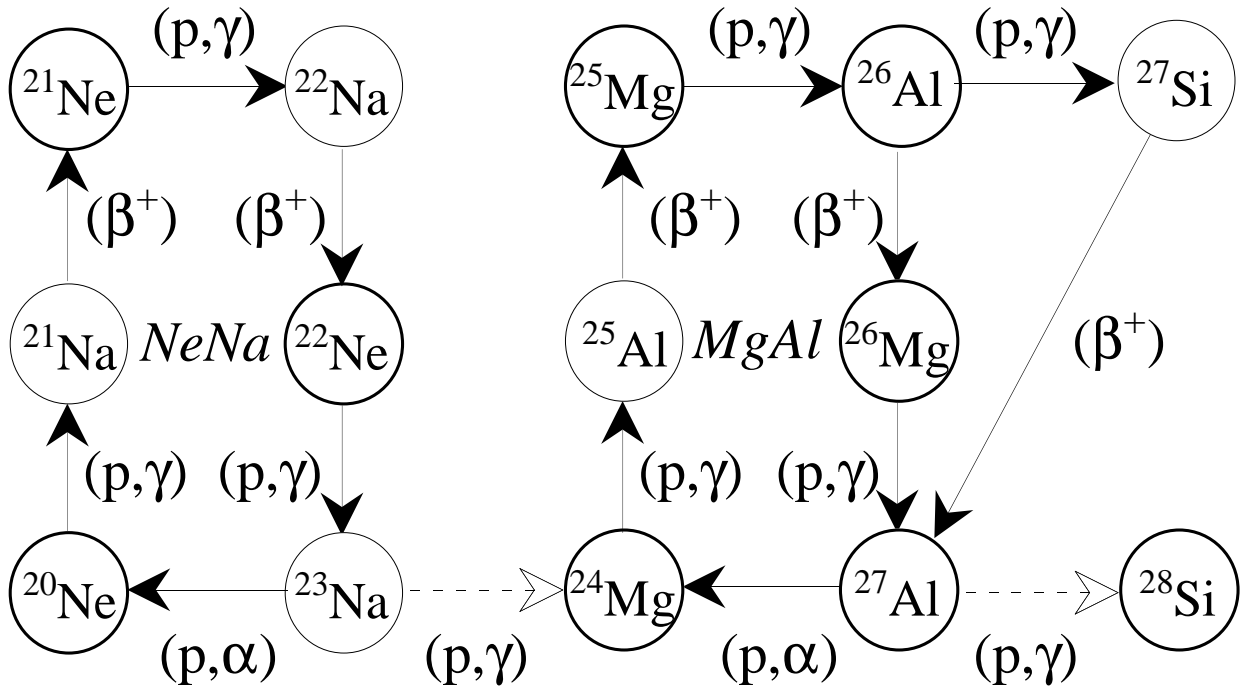


Fig. 9.— Reaction scheme of the NeNa- and MgAl-proton-capture cycles. The two reaction sequences leading to the creation of an α -particle are very similar to the CNO-I-cycle. (Figure courtesy of S. Goriely)

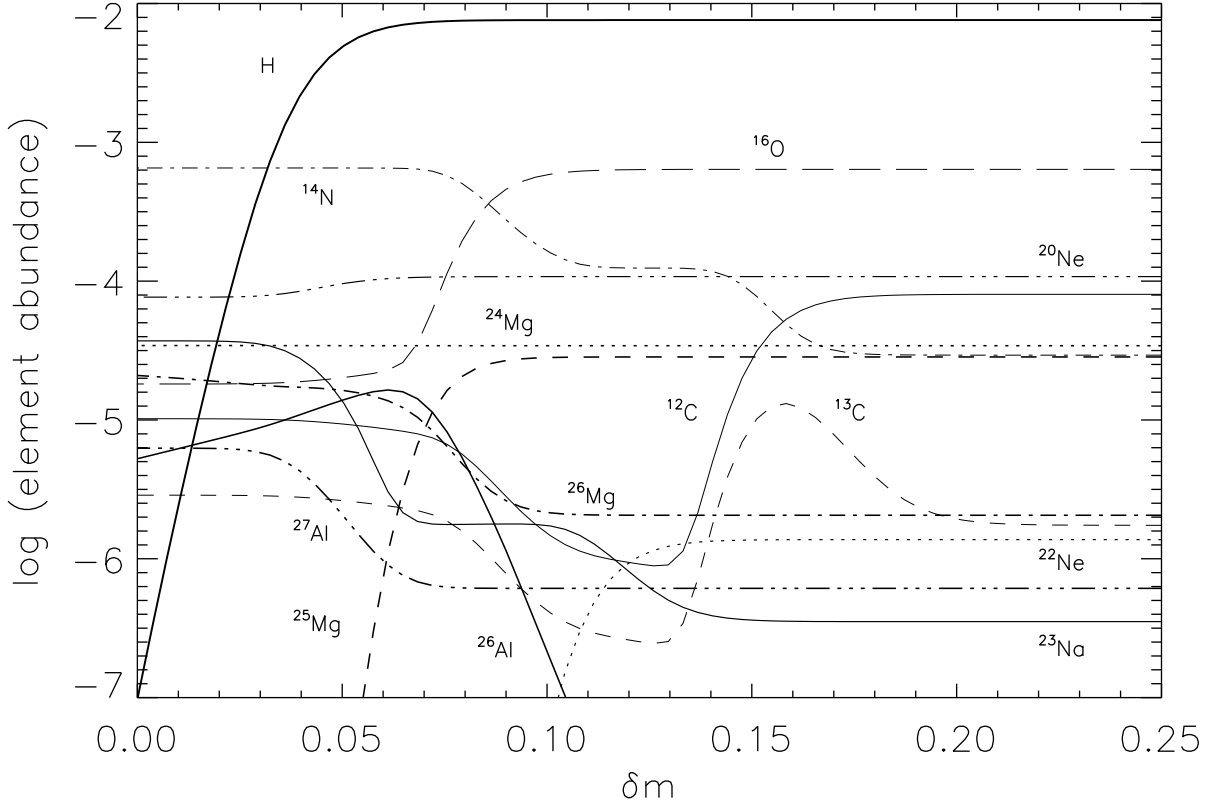


Fig. 10.— Abundance profiles (logarithmic mass fractions) within the hydrogen shell of an $0.8 M_{\odot}$ RGB-model of metallicity $[\text{Fe}/\text{H}] = -1.58$. For this model, taken from Denissenkov & Weiss (2001), $[\text{}^{25}\text{Mg}/\text{Fe}] = 1.2$ was assumed (primordial enrichment) and the standard NACRE-rates were used. The abscissa is in a relative mass coordinate δm , which is defined as 0 at the bottom of the H-shell and 1 at the bottom of the convective envelope. Plotted are the most important isotopes of the three proton-capture cycles, which are grouped by line thickness. Hydrogen has been scaled down by 1/100 to fit on the same scale. ${}^{26}\text{Al}$ refers to the ground state.

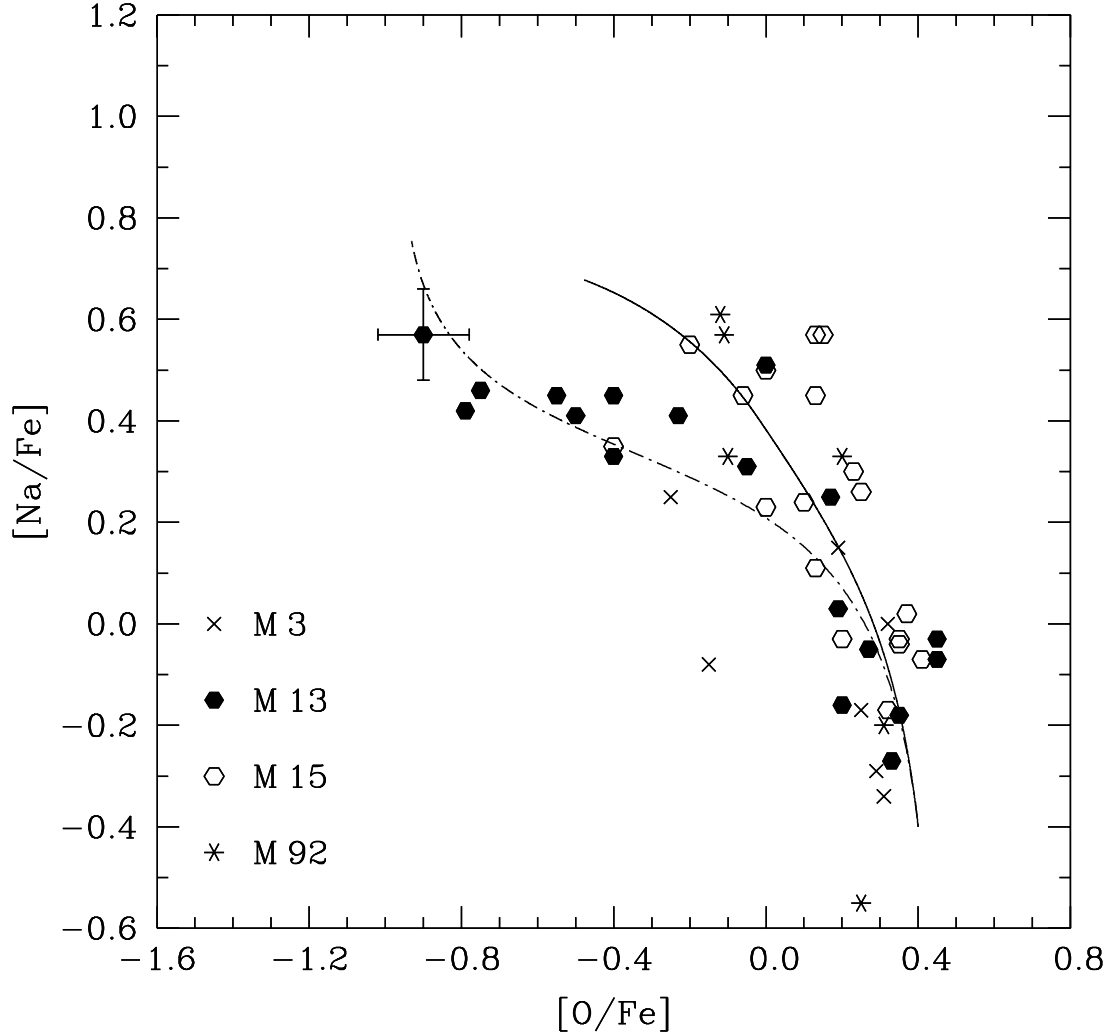


Fig. 11.— Observed Na-O-anticorrelation in a number of clusters (symbols; one with typical error bars), along with model predictions: the dot-dashed line is for mixing parameters of $2.5 \cdot 10^9 \text{ cm}^2 \text{ s}^{-1}$ for the constant of diffusive mixing and $\delta m = 0.06$ for penetration depth (Denissenkov et al. 1998); the solid line is for rotation-induced mixing following the model described in Denissenkov & Tout (2001) with an angular velocity at the bottom of the convective envelope of $8 \cdot 10^{-6} \text{ rad s}^{-1}$. Note that along the lines time increases as a parameter, while the data points are not necessarily ordered this way.

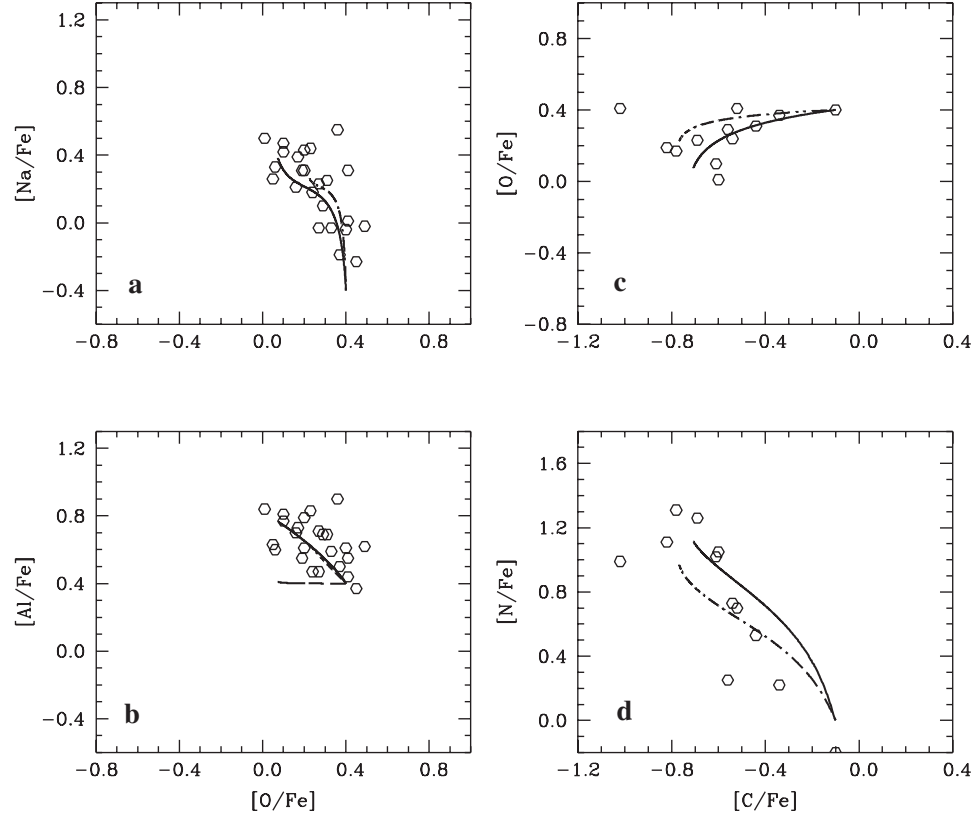


Fig. 12.— Observed element correlations in M4 (data by Ivans et al. 1999) and models (lines) by Denissenkov & Weiss (2001). The solid and dot-dashed lines correspond to two different penetration depths, $\delta m = 0.065$ and 0.075 respectively; the diffusive constant was

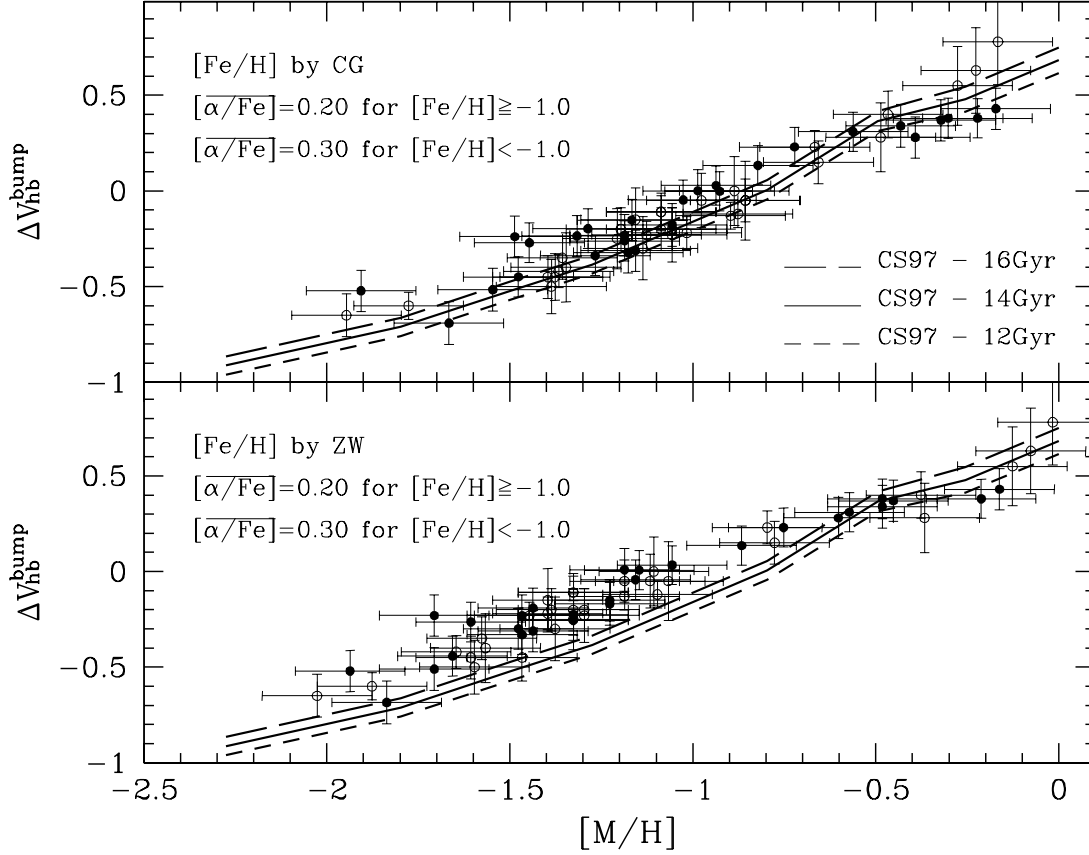


Fig. 13.— Comparison between the theoretical (CS97 models) and empirical values of $\Delta V_{\text{HB}}^{\text{Bump}}$ as a function of $[M/H]$. Full circles refer to the data by Zoccali et al. (1999), empty circles to the data by Ferraro et al. (1999). $[M/H]$ follows the Carretta & Gratton (1997) $[Fe/H]$ scale together with the labelled assumption about the α -enhancement (top panel). The bottom panel shows the same data but according to the Zinn & West (1984) $[Fe/H]$ scale.

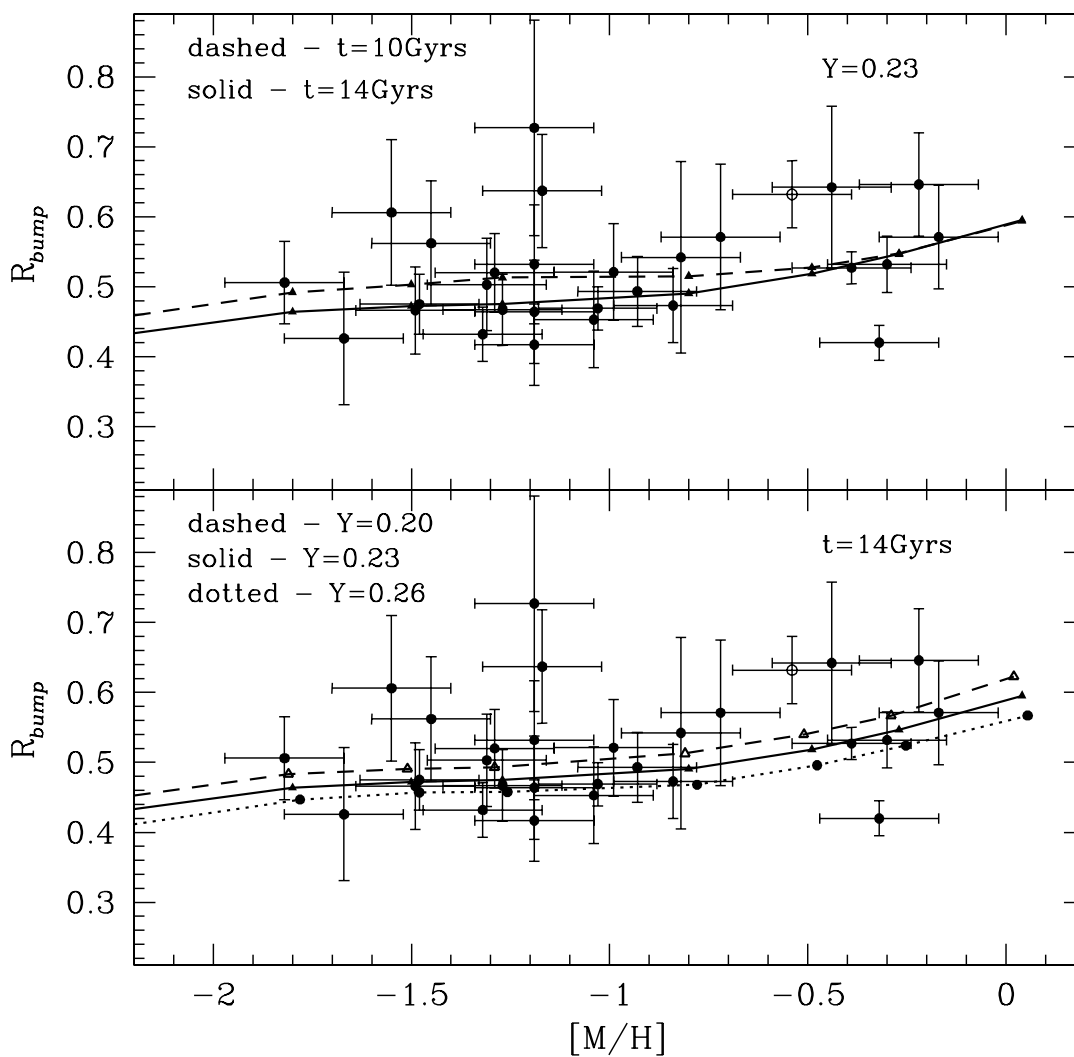


Fig. 14.— Comparison between observed (from Bono et al. 2001) and predicted (CS97 models) values of the R_{bump} parameter. The top panel shows the effect of varying age on the theoretical R_{bump} values; the bottom panel the effect of varying the initial He abundance. The open circle refers to the GC 47Tuc.

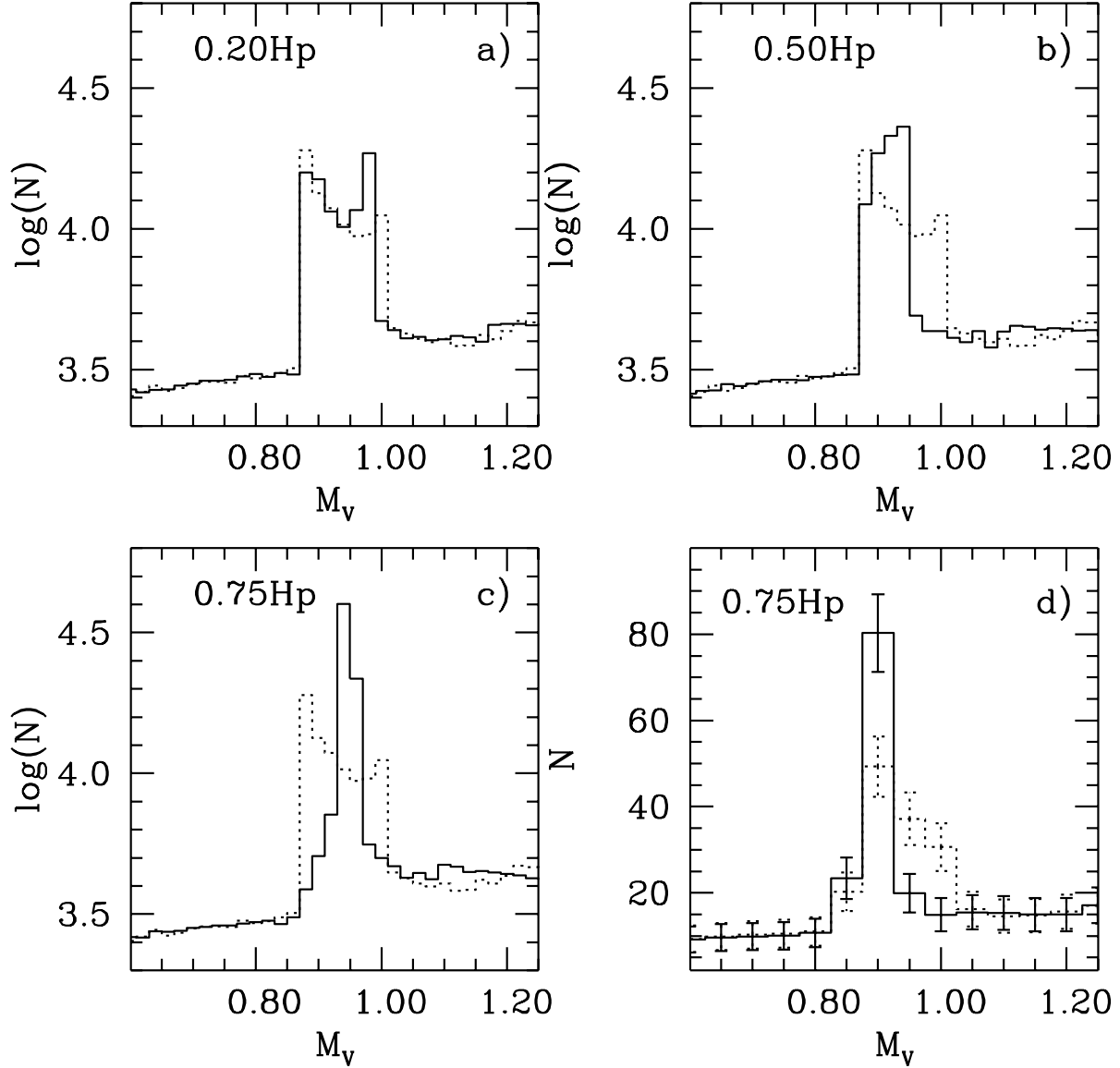


Fig. 15.— Panels a), b) and c) show a comparison between the LF from CS97 canonical models (dotted line) of $1M_{\odot}$ and $Z=0.006$, and LFs obtained accounting for various degrees of smoothing (as labelled) of the H-jump (solid lines). The bin size is 0.02 mag and all the LFs are normalized to the same arbitrary number of stars above the bump region. Panel d) shows the same comparison in the case of a smoothing of $0.75H_p$, but for the case of Monte-Carlo simulations with 200 stars within ± 0.20 mag of the bump peak, bin size of 0.05 mag and 1σ photometric errors of 0.015 mag; 1σ error bars on the stellar counts are also displayed. In each panel the LFs of the non-canonical models have been shifted in luminosity in order to match the bright end of the bump obtained from canonical models.

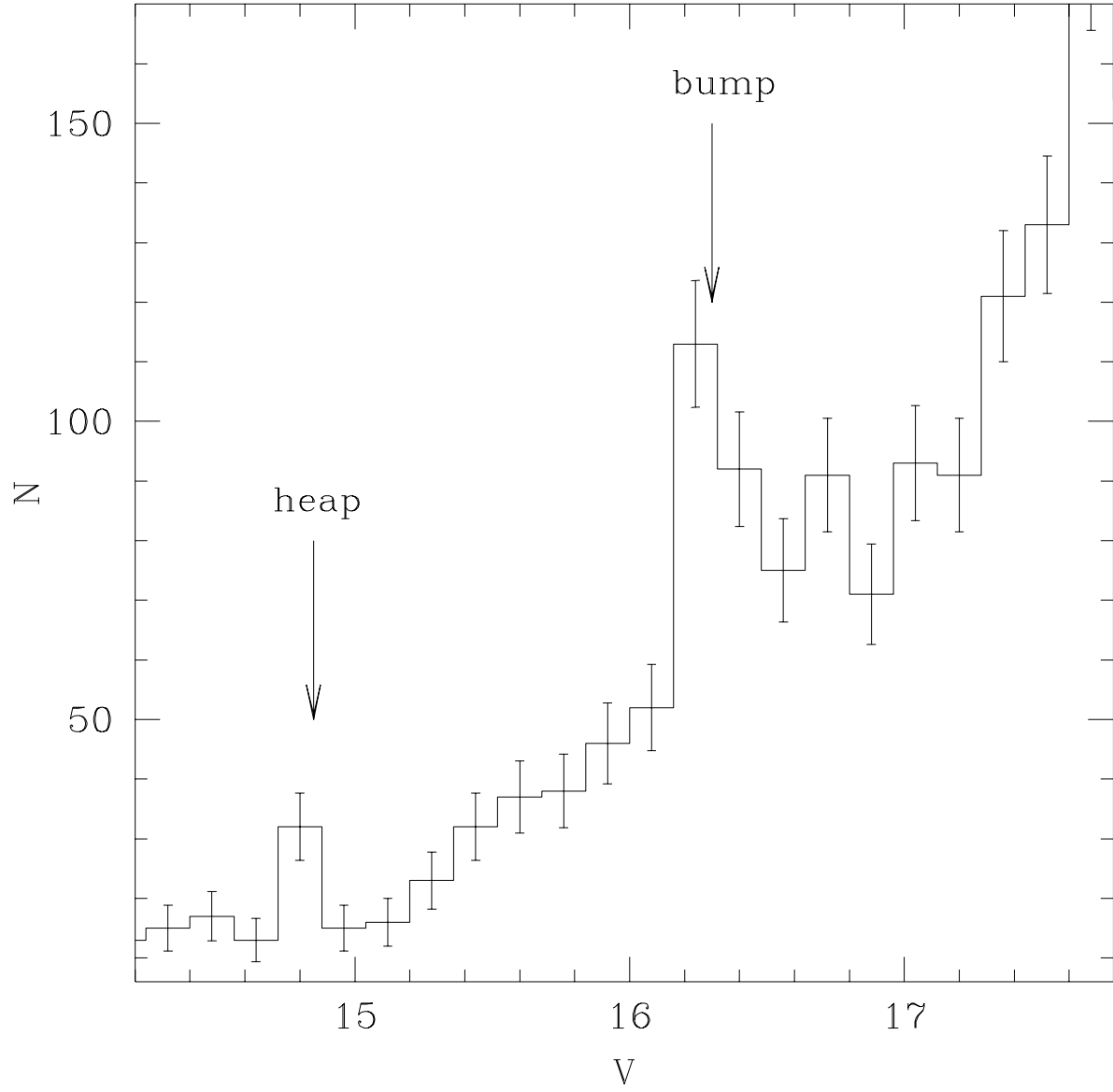


Fig. 16.— The LF of the RGB of NGC 2808. The arrows mark the position of the bump and the newly discovered heap.

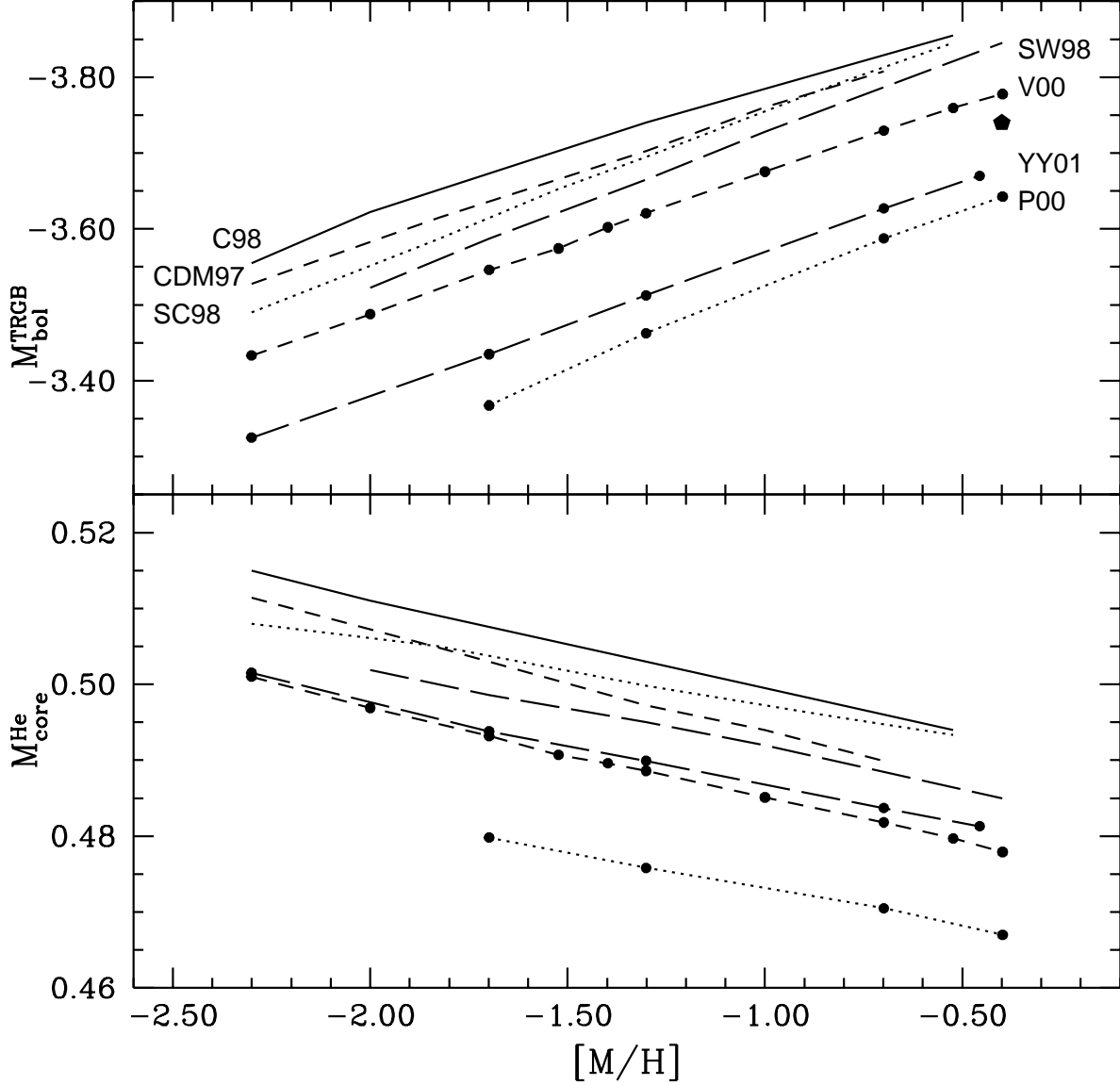


Fig. 17.— M_{bol}^{TRGB} - $[M/H]$ and M_{core}^{He} - $[M/H]$ (in solar mass units) relationships for $0.8M_{\odot}$ models from different authors. The meaning of the labels is as in Fig. 6, with the addition of Cassisi et al. (1998) – C98; Caloi, D’Antona & Mazzitelli (1997) – CDM97; Salaris & Cassisi (1998) – SC98. The filled symbol at $[M/H]=-0.4$ corresponds to the models by Salasnich et al. (2000).

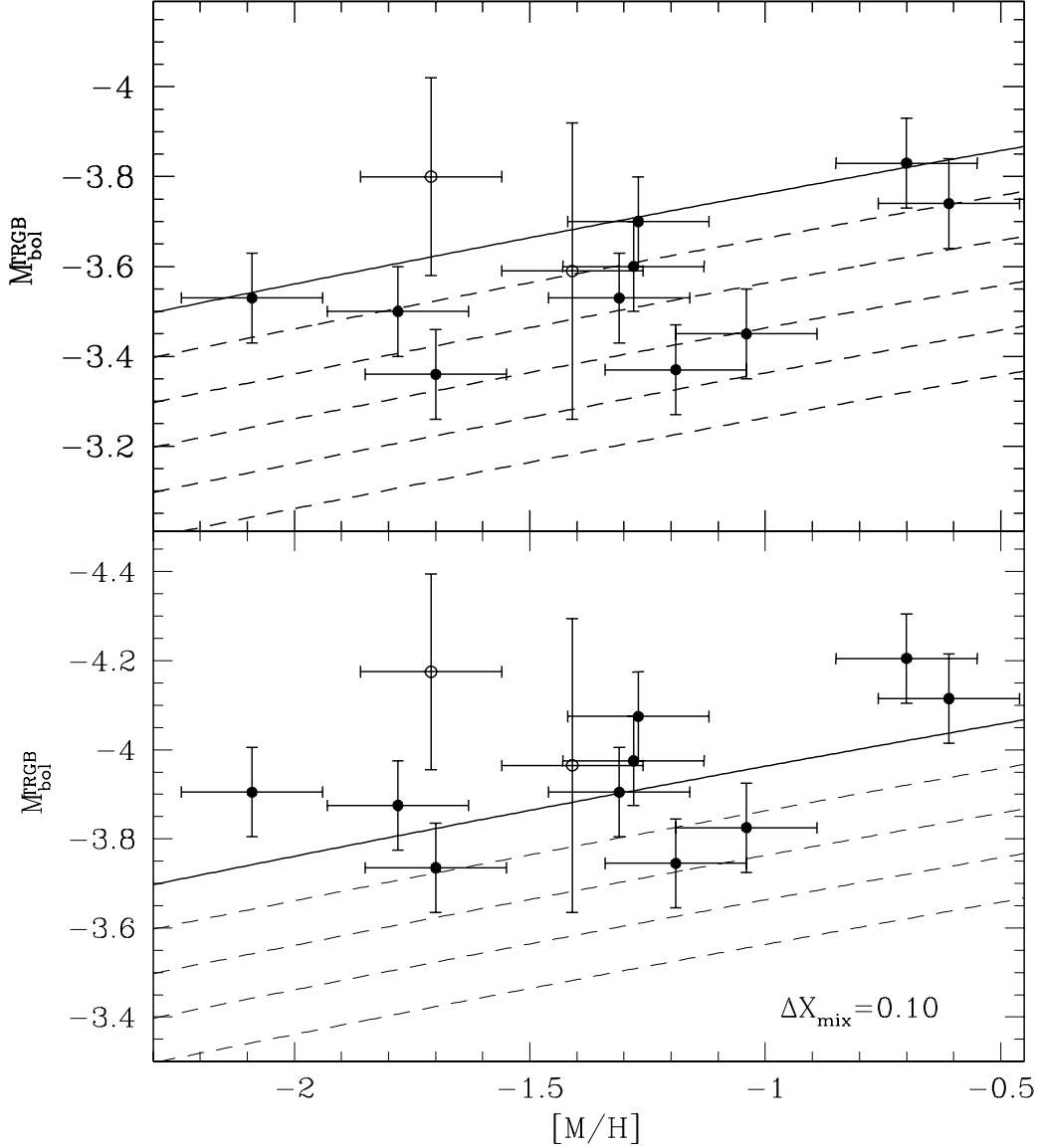


Fig. 18.— Comparison between the absolute bolometric magnitude of the brightest RGB star observed in selected GCs by FPC83 (full circles) and by Ferraro et al. (2000 – empty circles) corrected for the distance moduli obtained from the ZAHB models by CS98, and theoretical TRGB results by CS98 (solid line). The dashed lines represent the same theoretical relation but shifted in steps of 0.10 mag (top panel). The same is shown in bottom panel, but the theoretical TRGB value and the ZAHB distance scale account for an efficiency of envelope He mixing equal to $\Delta X_{\text{mix}} = 0.10$ (see text for details).